UNIVERSITY OF CRETE, DEPARTMENT OF BIOLOGY

The role of NER factors in mouse development and disease

Ismene Karakasilioti

PhD thesis

Heraklion, 2014

This research has been conducted at the Institute of Molecular Biology and Biotechnology, Foundation of Research and Technology (IMBB-FORTH), under the supervision of Dr. Prof. George A. Garinis, Laboratory of Mammalian Physiology and Genome Instability.

This research has been co-financed by the European Union (European Regional Development Fund - ERDF) and Greek national funds through the Operational Program ‘Competitiveness and Entrepreneurship’ OPCEII of the General Secretariat of Research and Technology (GSRT). Research Funding program ‘Cooperation’ - Development of a National Network for Genomic Research: Methodological approaches for Systems Biology.

Ismene Karakasilioti acknowledges personal funding from the Maria Michail Manassakis scholarship program.

Τριμελής συμβουλευτική επιτροπή

Δέσποινα Αλεξανδράκη: Αναπληρώτρια Καθηγήτρια, τμήμα Βιολογίας, Πανεπιστήμιο Κρήτης και συνεργαζόμενο μέλος ΔΕΠ, Ινστιτούτο Μοριακής Βιολογίας και Βιοτεχνολογίας-ΙΤΕ

Γιώργος Γαρίνης : Αναπληρωτής Καθηγητής, τμήμα Βιολογίας, Πανεπιστήμιο Κρήτης και συνεργαζόμενο μέλος ΔΕΠ, Ινστιτούτο Μοριακής Βιολογίας και Βιοτεχνολογίας-ΙΤΕ

Δημήτρης Τζαμαρίας: Αναπληρωτής Καθηγητής, τμήμα Βιολογίας, Πανεπιστήμιο Κρήτης.

Επταμελής εξεταστική επιτροπή

Δέσποινα Αλεξανδράκη: Αναπληρώτρια Καθηγήτρια, τμήμα Βιολογίας, Πανεπιστήμιο Κρήτης και συνεργαζόμενο μέλος ΔΕΠ, Ινστιτούτο Μοριακής Βιολογίας και Βιοτεχνολογίας-ΙΤΕ

Γιώργος Γαρίνης : Αναπληρωτής Καθηγητής, τμήμα Βιολογίας, Πανεπιστήμιο Κρήτης και συνεργαζόμενο μέλος ΔΕΠ, Ινστιτούτο Μοριακής Βιολογίας και Βιοτεχνολογίας-ΙΤΕ

Δημήτρης Τζαμαρίας: Αναπληρωτής Καθηγητής, τμήμα Βιολογίας, Πανεπιστήμιο Κρήτης

Δημήτρης Καρδάσης: Καθηγητής, Ιατρική Σχολή, Πανεπιστήμιο Κρήτης και συνεργαζόμενο μέλος ΔΕΠ, Ινστιτούτο Μοριακής Βιολογίας και Βιοτεχνολογίας-ΙΤΕ

Αριστείδης Ηλιόπουλος: Καθηγητής, Ιατρική Σχολή, Πανεπιστήμιο Κρήτης και συνεργαζόμενο μέλος ΔΕΠ, Ινστιτούτο Μοριακής Βιολογίας και Βιοτεχνολογίας-ΙΤΕ

Ιωσήφ Παπαματθαιάκης: Καθηγητής, τμήμα Βιολογίας, Πανεπιστήμιο Κρήτης και συνεργαζόμενο μέλος ΔΕΠ, Ινστιτούτο Μοριακής Βιολογίας και Βιοτεχνολογίας-ΙΤΕ

Χαράλαμπος Σπηλιανάκης: Επίκουρος Καθηγητής, τμήμα Βιολογίας, Πανεπιστήμιο Κρήτης και συνεργαζόμενο μέλος ΔΕΠ, Ινστιτούτο Μοριακής Βιολογίας και Βιοτεχνολογίας-ΙΤΕ

Ευχαριστίες

Με μεγάλη μου χαρά, ολοκληρώνω τις σπουδές μου και ταυτόχρονα, τη δεκαετή και πλέον παραμονή μου στην Κρήτη. Θέλω, λοιπόν, να ευχαριστήσω όλους τους καθηγητές μου και ιδιαίτερα τα μέλη της τριμελούς συμβουλευτικής επιτροπής του διδακτορικού μου και όλους όσοι με συμβούλεψαν κατά τη διάρκεια της διατριβής μου. Ξεχωριστή σημασία για μένα είχε η συνεργασία μου με τον επιβλέποντα της διατριβής μου, Γιώργο Γαρίνη. Ο Γιώργος διέθεσε πολύ χρόνο, προσπάθεια, γνώση και αστείρευτη ενέργεια, ώστε να με καθοδηγήσει όσο το δυνατόν πληρέστερα προς την ολοκλήρωση της παρούσας έρευνας. Για μένα, τα τελευταία τεσσερισήμισι χρόνια υπήρξαν πολύ παραγωγικά, γεμάτα εμπειρίες και με πολλές χαρές. Σε αυτό συνέβαλαν όλοι οι συνεργάτες, εντός και εκτός της ομάδας του Γιώργου, με τους οποίους είχα τη χαρά να δουλέψω. Θέλω να ευχαριστήσω ιδιαίτερα τον Τεό για την προθυμία, την αισιοδοξία και την υπομονή του όλα αυτά τα χρόνια και την Ειρήνη, με την οποία δουλέψαμε παράλληλα και με επιμονή, ώστε να ξεπεράσουμε τις πολλές δυσκολίες που συναντήσαμε ως μέλη μιας νέας ομάδας. Ξεχωριστά ευχαριστώ ανήκουν και στην Τζωρτζίνα, της οποίας η βοήθεια υπήρξε καθοριστική σε πολλαπλά επίπεδα. Τέλος, ευχαριστώ τον Ζήση, τη Μαρία, την Άννα και όλα τα νέα και παλιά μέλη του εργαστηρίου για τις συζητήσεις, τα γέλια, τα τραγούδια και όλες τις αναμνήσεις που παίρνω μαζί μου. Θα είστε πάντα στη σκέψη μου και θα μου λείψετε πολύ.

Σε προσωπικό επίπεδο, η περίοδος του διδακτορικού υπήρξε διαφωτιστική, μια διαδικασία ωρίμανσης και αυτογνωσίας. Η στήριξη της οικογένειάς μου υπήρξε καταλυτική σε αυτή την πορεία, διότι μου επέτρεψε να αναζητώ, να επιλέγω και να προχωρώ προς την κατεύθυνση που θέλω, χωρίς επίκριση και αμφισβήτηση. Τους ευχαριστώ όλους για το ενδιαφέρον και την αγάπη που μου δείχνουν όλα αυτά τα χρόνια. Τέλος, θέλω να ευχαριστήσω τους φίλους μου που κάνουν τη ζωή μου πλούσια και χαρούμενη. Την Πασχαλιά, τον Σωτήρη, τον Αντρέα, τη Νίκη, την Μαργαρίτα. Και τους δύο ανθρώπους που κάνουν τη μέρα μου ξεχωριστή, ακόμη κι όταν είναι μακριά. Την Πολύμνια, που από το πρώτο έτος των σπουδών μας μου προσφέρει απλόχερα τη φιλιά της και με βοηθά να ανακαλύπτω ποια είμαι. Τον Γιάννη, που μου θυμίζει ποια είμαι και που έχει βρει τον τρόπο να στέκεται δίπλα μου, ένα βήμα μπροστά ή πίσω, όταν χρειάζεται.

…

Τί νὰ πεῖς, δὲν ξέρεις.
Δύσκολα εἶναι στὴν ἀρχή.

Γιατὶ δὲν εἶναι, κοριτσάκι,
νὰ μάθεις μόνο
ἐκεῖνο ποὺ εἶσαι,
ἐκεῖνο ποὺ ἔχεις γίνει.

Εἶναι νὰ γίνεις
ὅ,τι ζητάει
ἡ εὐτυχία τοῦ κόσμου

Στον μπαμπά μου

Table of contents

Περίληψη

Ο ρόλος της γενωμικής αστάθειας στην εμφάνιση ιστο-ειδικής παθολογίας σε ασθενείς και ποντίκια που φέρουν μεταλλαγές στα γονίδια του μηχανισμού εκτομής νουκλεοτιδίων δεν είναι γνωστός και υποθέτουμε πως υπάρχουν ιστο-ειδικές αποκρίσεις κατά επιβλαβών καταστάσεων. Κάνοντας χρήση του Cre/LoxP γενετικού συστήματος και του Fabp4-aP2 υποκινητή που εκφράζεται ειδικά στον λιπώδη ιστό, αναπτύξαμε έναν ποντικό μοντέλο με ιστο-ειδική απώλεια λειτουργίας για το *Ercc1* γονίδιο στο λίπος. Τα aP2-*Ercc1*$^{-/-}$ ποντίκια αναπτύσσονται φυσιολογικά και δεν διαφέρουν από τα ποντίκια αναφοράς. Από την ηλικία των τριών μηνών, τα aP2-*Ercc1*$^{-/-}$ ποντίκια έχουν λιγότερο βάρος, οι αποθήκες λίπους τους είναι σημαντικά μικρότερες και εμφανίζουν συνολική απώλεια του λιπώδους ιστού. Πειράματα ηλεκτρονικής μικροσκοπίας σάρωσης αποκάλυψαν έναν δραματικό εκφυλιστικό φαινότυπο που περιλαμβάνει ρήξη της βασικής μεμβράνης, απώλεια λιποκυττάρων και εκτενή ίνωση. Ο φαινότυπος αυτός συνοδεύεται από επιπλοκές στον μεταβολισμό που εμφανίζονται συνήθως όταν τα λιποκύτταρα είναι δυσλειτουργικά. Ανάλυση της γονιδιακής έκφρασης του λιπώδους ιστού από αγρίου τύπου και *Ercc1*$^{-/-}$ ποντίκια κατέδειξε 2200 διαφορικά εκφραζόμενα γονίδια που ανήκουν σε μονοπάτια όπως: απόκριση σε διπλές θραύσεις της DNA έλικας, προ-φλεγμονώδης σηματοδότηση και σηματοδότηση από πυρηνικούς υποδοχείς και αυξητικούς παράγοντες. Μια ομάδα γονιδίων που αποκρίνονται στις διπλές θραύσεις της DNA έλικας υπερεκφράζονται στον λιπώδη ιστό των aP2-*Ercc1*$^{-/-}$ ποντικιών και κάποια από αυτά συγκεντρώνονται σε πυρηνικές εστίες, η παρουσία των οποίων υποδηλώνει απόκριση σε DNA αλλοιώσεις. Στον λιπώδη ιστό των aP2-*Ercc1*$^{-/-}$ ποντικιών πολλά λιποκύτταρα πεθαίνουν μέσω νέκρωσης και γύρω τους σχηματίζονται στεφανιαίες δομές, που περιλαμβάνουν προ-φλεγμονώδη λευκοκύτταρα. Η παρατήρηση αυτή σηματοδοτεί την *in vivo* συσχέτιση της

απόκρισης σε DNA αλλοιώσεις με τη φλεγμονώδη απόκριση. Χρησιμοποιώντας ένα *in vitro* σύστημα κυτταρικών καλλιεργειών, αποδείξαμε ότι η απώλεια της *Ercc1*, καθώς και οι ίδιες οι DNA αλλοιώσεις, δρουν με κυτταρικά αυτόνομο τρόπο, ώστε να επάγουν την ATM-εξαρτώμενη αντιστροφή της καταστολής υποκινητών που σχετίζονται με την προ-φλεγμονώδη απόκριση, σε ινοβλάστες που έχουν υποστεί διαφοροποίηση προς λιποκύτταρα. Συνολικά, τα δεδομένα αυτά υποστηρίζουν την ύπαρξη ενός ενδογενούς σήματος που εξαρτάται από τις DNA αλλοιώσεις και επάγει μια αυτό-φλεγμονώδη απόκριση στον λιπώδη ιστό, η οποία τελικά οδηγεί στη λιποδυστροφία που παρατηρείται στη NER προγηρία.

Abstract

How DNA damage triggers the onset of tissue-specific pathology in patients and mice carrying defects in nucleotide excision repair (NER) remains an intriguing question arguing for tissue-specific responses against deleterious threats. Using a Cre/LoxP strategy, we have generated an adipose tissue-specific *Ercc1* knock-out mouse, employing the Fabp4-aP2 driver, which is specifically expressed in adipose. The aP2-*Ercc1*$^{-/-}$ mice develop normally into adulthood and are indistinguishable to their littermate controls. From three months of age onwards the aP2-*Ercc1*$^{-/-}$ mice fail to gain weight and the majority of their adipose tissue depots are smaller, ultimately presenting generalized fat depletion. Scanning electron microscopy revealed a gross degenerative phenotype, including basement membrane rupture, adipocyte depletion and extensive fibrosis, accompanied by metabolic abnormalities usually observed when adipocytes are dysfunctional. Comparison of gene expression data from wt and *Ercc1*$^{-/-}$ adipose tissues showed 2200 genes that are differentially expressed with over-represented pathways including: the double-strand break response, pro-inflammatory signalling, nuclear receptor and growth factor signalling. A number of DSB responsive genes are up-regulated in the aP2-*Ercc1*$^{-/-}$ adipose and a subset forms nuclear foci, a hallmark of the DNA damage response. In the aP2-*Ercc1*$^{-/-}$ EWAT a large number of adipocytes undergo necrotic death and form crown-like structures with infiltrating pro-inflammatory leukocytes, establishing an *in vivo* link between DDR and the inflammatory response. Using an *in vitro* cell culture system, we document that the Ercc1 defect as well as DNA damage *per se* can act in a cell-autonomous manner and induce a pro-inflammatory response by de-repressing gene promoters, when mouse embryonic fibroblasts are

exposed to an adipogenic regime, a response that is not observed upon ATM inhibition. Collectively, these data support the idea of an endogenous DNA damage-dependent signal that induces an auto-inflammatory response in the adipose tissue, ultimately leading to lipodystrophy in NER progeria.

Key words: DNA repair, adipose, inflammation, promoter de-repression, metabolism

Introduction

All macromolecules e.g. proteins, lipids or nucleic acids are subject to hazardous threats of endogenous – metabolic by-products – or exogenous origin – solar irradiation, chemical compounds – that alter their chemical structure resulting in their gradual degradation. Although this process is fundamentally indiscriminate in nature, chemical or structural alterations in the DNA are, in general, considered more adverse than those seen in proteins, lipids or RNA. Unlike DNA, all other macromolecules can be replaced once damaged, provided that the initial genomic information remains intact (Garinis *et al*. 2008). Indeed, preservation of genetic information is of prime importance to all living systems. Nevertheless, the integrity of the genome is continuously threatened by a variety of environmental and endogenous agents that damage the DNA, as well as by intrinsic instability of chemical bonds in DNA itself. Both endogenous – reactive oxygen species or other secondary metabolites – and exogenous – UV light, chemical compounds in foods or smoke – sources generate numerous DNA insults, such as the DNA double strand breaks (DSBs), intra- or inter-strand DNA cross links (ICLs), base modifications or UV-induced photoproducts and bulky pyrimidine dimers (Hoeijmakers, 2001). Eventually, the effects of distinct types of lesions diverge with respect to helix distortion, ability to pause or obstruct DNA replication, block ongoing transcription or else hamper the battery of repair systems and other caretakers that continuously safeguard the genome. Mutagenic lesions, i.e. spontaneous deaminations, depurinations and certain oxidized bases, are predominantly responsible for mutations and contribute to carcinogenesis. On the other hand, cytotoxic or cytostatic lesions (e.g. double strand breaks, UV-induced lesions, DNA interstrand cross links [ICLs], uncapped telomeres and certain oxidized

bases) are thought to predominantly cause apoptosis or senescence, respectively, thereby contributing to aging. Alternatively, failure of the repair mechanisms to correct the damaged DNA strand leads to permanent cell cycle arrest or apoptosis (de Boer and Hoeijmakers, 2000; Citterio *et al*. 2000). DNA breaks are primarily repaired by homologous recombination (HR), a process that utilizes undamaged sister chromatids as template to correct the DNA strand that contains the break, or by a less accurate reaction, non-homologous end joining (NHEJ), which ligates the two ends of a DNA break (West, 2003). ICLs are removed by ICL repair, a process that is coordinated by Fanconi Anemia (FA) proteins and leads to the excision of the DNA cross-link by endonucleases, such as Xeroderma Pigmentosum group F (XPF), Structure-specific endonuclease subunit SLX1 or Crossover junction endonuclease MUS81 (Kottemann and Smogorzewska, 2013). Small structural base modifications are repaired by Base Excision Repair (BER), whereas Nucleotide Excision Repair (NER) removes bulky lesions that distort the double helix, such as UV-induced cyclobutane pyrimidine dimers (CPDs) and 6-4 photoproducts (6-4PPs) (Friedberg, 2001). Despite being highly complex, DNA repair systems operate within constrains. Excessive DNA damage load exceeds their repair capacity and as a result, DNA damage accumulates with time. Mutations in genes that encode for DNA repair factors spur DNA damage accumulation, which results in genomic instability that ultimately leads to cancer or ageing (de Boer and Hoeijmakers, 2000).

The Nucleotide Excision Repair pathway

Nucleotide Excision Repair (NER) represents a highly conserved, complex pathway that is primarily involved in removing helix-distorting lesions from the DNA (Hoeijmakers, 2001). NER employs approximately 30 protein factors which operate in a step-wise

manner to recognise, verify and correct the damaged nucleotides (**Figure 1**). Depending on how the damage is recognized, NER is divided into two sub-pathways. In Global Genome NER (GG-NER), XPC, in complex with RAD23B and Centrin 2 (CETN2), scan the genome for helix distorting lesions (Masutani *et al*. 1994; Nishi *et al*. 2005) and this is facilitated by the UV-damaged DNA-binding proteins 1 and 2 (UV-DDB1, 2) (Lagerwerf *et al*. 2011). In Transcription-Coupled NER (TC-NER), RNA polymerase II (RNA Pol II) itself activates the downstream pathway, when it is physically blocked by a lesion in the actively transcribed part of the genome (Hanawalt, 2002). Activation of TC-NER by RNA Pol II requires the NER factors Cockayne Syndrome group A and B proteins (CSA, CSB) (Spivak *et al*. 2002; Laine and Egly, 2006). CSB, a DNA-dependent ATPase, co-localizes with stalled RNA Pol II and is instrumental in recruiting chromatin remodelling factors, such as the histone acetyltransferase p300 and downstream NER proteins (Fousteri *et al*. 2006). CSA participates in an E3-ubiquitin ligase complex together with DDB1, Cullin 4A (CUL4A) and Ring-box protein 1 (RBX1), which has been implicated in ubiquitylating CSB, RNA Pol II, and proximal histones, upon UV-induced DNA lesions (Saijo, 2013). Recently, it was shown that an additional factor, UV-sensitive syndrome protein A (UV-SSA), is involved in stabilizing CSB by recruiting the de-ubiquitylase USP7 to the stalled RNA Pol II (Schwertman *et al*. 2012). Upon lesion recognition either by GG- or TC-NER, the general transcription factor TFIIH unwinds the double helix locally, with its helicase subunits XPB and XPD, and single-stranded DNA is stabilized by replication protein A (RPA), in conjunction with XPB and XPD (Oksenych *et al*. 2009). RPA-mediated stabilization of the DNA bubble around the lesion triggers the recruitment of structure-specific endonucleases that cleave the damaged strand to remove the damage-containing oligonucleotide. Excision Repair Cross-Complementing group protein 1 (ERCC1) in complex with XPF, incise the 5’ end of the DNA bubble, whereas

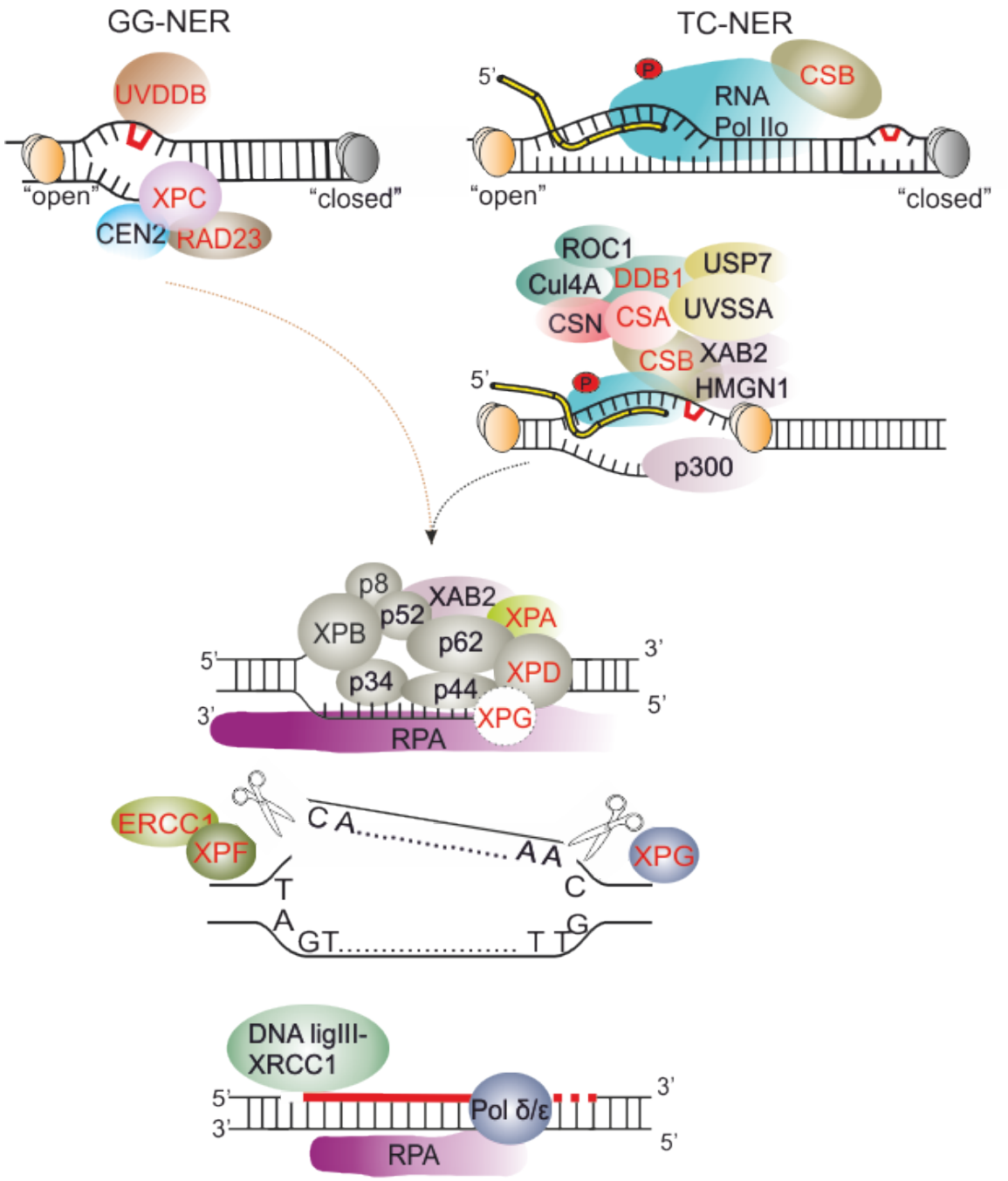

Figure 1 The Nucleotide Excision Repair pathway. Global genome NER (top left) recognizes and removes helix-distorting lesions throughout the genome and Transcription-coupled NER (top right) selectively removes similar lesions from the actively transcribed part of the genome. Following damage recognition, the two sub-pathways converge into a common mechanism that involves unwinding of the double helix around the lesion, stabilization and excision of the damage-containing DNA fragment and gap filling and ligation of newly synthesized DNA. Protein names colored in red depict the availability of mouse models carrying a defect in the corresponding gene. (Adapted from Kamileri *et al*. 2012)

at the 3' end, the incision event is performed by XPG (Overmeer *et al*. 2011). The excision event creates a single-stranded gap that is filled by DNA polymerases δ and ε. Finally, DNA ligases I and III together with X-ray Repair Cross-Complementing group protein 1 (XRCC1) ligate the newly synthesized DNA fragment back to the DNA strand (Moser *et al*. 2007).

NER syndromes and related mouse models

DNA repair pathways are highly conserved since all cells need to employ them to counteract the adverse effects of a damaged genome. This, together with the fact that mutations in genes that code for repair factors cause severe defects and dramatic phenotypes to individuals that carry them, underscore the relevance of genome maintenance to a healthy lifespan (van Gent *et al*. 2001). Mutations in genes that code for NER factors cause three major, life-threatening human disorders: Xeroderma Pigmentosum (XP), Cockayne Syndrome (CS) and Trichothiodystrophy (TTD). XP patients carry mutations in *Xp-a* to *g* genes and develop skin cancer in a >1000 fold higher incidence (de Boer and Hoeijmakers, 2000). Mutations in *Csa* (*Ercc8*) and *Csb* (*Ercc6*) cause CS, whereas mutations in *Xpb, Xpd* and *Ttd-a* lead to the development of TTD syndrome. These mutations are not cancer-prone; they are related to the manifestation of a complex pathology that includes premature ageing (progeroid) symptoms in several organs. These are: sarcopenia, neurodegeneration, kyphosis and fat depletion (Andressoo *et al*. 2006). Although such cases are rare, patients with combined manifestation of XP/CS have also been described and have been linked to distinct mutations in *Xpb, Xpd* and *Xpg* genes (Laugel *et al*. 2010). More recently, Niedernhofer and colleagues described a *Xpf*-deficient patient that does not manifest XP symptoms, but

rather develops neurological, hematopoietic and musculoskeletal defects, which led them to describe a new progeroid syndrome, XFE (Niedernhofer *et al*. 2006). Even more, patients that carry identical mutations in the *Csb* or *Xpb* genes, but manifest distinct clinical symptoms have also been observed. In one case, siblings carried a silent C2830T and a non-sense C2282T point mutation in the *Csb* gene and manifested a variant form of XP, named DeSanctis-cacchione. The same mutant *Csb* allele had been described to cause the classical form of CS in another patient (Colella *et al*. 2000). Similar observations were made for a mis-sense mutation in the *Xpb* gene, which in one case caused the manifestation of mild XP/CS, whereas in two different patients, it led to manifestation of mild XP (Oh *et al*. 2006). It is apparent that NER defects, possibly due to their mechanistic complexity, can cause a wide range of symptoms and the manifestation of diverse syndromes that may develop in a congenital manner or at later stages in life. This remarkable genetic heterogeneity has made it difficult to clearly connect particular NER genes to symptoms observed in the clinic. The mouse mutants that have been developed for several of the NER factors (**Figure 1**; gene names in red) provide valuable tools towards understanding the mechanistic and phenotypic complexity of the abovementioned syndromes (Hasty *et al*. 2003).

NER deficient mouse models have been studied for more than two decades and allowing us to gain insight into the molecular pathways affected by genomic instability, as well as the tissue-specific and systemic responses that are observed upon NER inactivation (Schumacher *et al*. 2008; Garinis *et al*. 2008). Several attempts to generate knock-out mouse models that bear null homozygous alleles for the TFIIH subunits XPD, XPB and TTD-A, which are involved in NER, resulted in early embryonic lethality (de Boer *et al*. 1998; Andressoo *et al*. 2009; Theil *et al*. 2013). However, mouse models bearing non-

lethal mutations in these genes (*Xpd*^{TTD} and *Xpd*^{XPCS}), and which mimic patients' mutant alleles, were viable and presented disease symptoms greatly mimicking the corresponding syndromes (de Boer *et* al. 2002; Andressoo *et al*. 2006b). The *Xpd*^{TTD} mutant mice carry a *XPD* point mutation found in TTD patients and develop progeroid symptoms, including cachexia and kyphosis, as well as brittle hair, the hallmark of TTD patients (de Boer *et al*. 2002). The *Xpd*^{XPCS} mouse model develops UV-induced skin cancer, but also shows mild developmental and neurological abnormalities, also observed in corresponding patients (Andressoo *et al*. 2006b). Mouse models bearing null homozygous mutant alleles for other NER factors also exist. The *Ercc1*$^{-/-}$ mice show severe growth retardation, both as embryos and postnatally, and develop a very complex pathology, including ataxia, liver and kidney defects, cachexia, kyphosis and sarcopenia, symptoms that resemble the *Xpf*/*Ercc1*-deficient patients (Weeda *et al*. 1997; Niedernhofer *et al*. 2006; Jaspers *et al*. 2007).

Growth and lifespan are regulated by anabolic pathways, such as the insulin-like growth factor 1/growth hormone (IGF1/GH axis) and the molecular target of rapamycin (mTOR) (Kenyon, 2010). Growth hormone is produced and secreted by the pituitary in response to hormonal signals from the hypothalamus. In an endocrine manner, it acts on peripheral organs, where it induces the expression of IGF1. IGF1 is mainly produced and is secreted into the blood stream by the liver. This in turn, triggers glucose uptake and growth in the soma (Clemmons, 2007). The somatotropic axis has been shown to regulate lifespan also in worms and flies (Kenyon, 2006). Microarray experiments in the livers of 15-day old *Ercc1*$^{-/-}$ compared to wild type mice revealed lower expression levels of genes that are associated with the three major hormonal axes of the animal, namely the somatotropic, lactotropic and thyrotropic axis, whereas genes that participate in glycogen and lipid

synthesis, as well as in oxidative stress response were overexpressed in the *Ercc1*$^{-/-}$ livers. IGF1, basal glucose and insulin were detected in lower amounts in the sera of these mice, further supporting the dampening of the growth axes observed in the transcriptome profile. However, the finding that glycogen and triacylglycerols are stored in the livers of these mice, while they are hypoinsulinaemic represents a paradox. It is possible that the Ercc1 defect in the liver induces energy storage in the form of lipids and glycogen independent of insulin action (Niedernhofer *et al*. 2006). Similar defects have been described in another growth-deficient model, the *Csb*$^{m/m}$/*Xpa*$^{-/-}$ mouse, which also dies prematurely (van der Pluijm *et al*. 2007). Genetic deletion of *Xpg* (Harada *et al*. 1999) and *Xpf* (Tian *et al*. 2004) also resulted in growth retardation and premature death. The single mutant mice *Csb*$^{m/m}$ (van der Horst *et al*. 1997) and *Xpa*$^{-/-}$ (de Vries *et al*. 1995; Nakane *et al*. 1995) which are otherwise susceptible to UV-induced skin tumours, do not manifest growth defects or premature death. Collectively, these findings suggest that the DNA repair defect alone does not fully explain the phenotypic heterogeneity observed in NER deficient mouse models.

In an attempt to link the DNA damage response to the down-regulation of the somatotropic axis, Garinis and colleagues (2009) showed that this effect is cell autonomous and can be recapitulated *in vitro* upon exposure of primary mouse embryonic fibroblasts and chondrocytes to exogenous DNA damaging agents. However, they did not manage to provide a mechanistic link between DNA repair factors and the down-regulation of gene expression (Garinis *et al*. 2009). Following this, it was later shown that specific NER factors are recruited together with RNA Pol II and the general transcription factor TFIID on the promoters of genes that are important for postnatal murine development in the liver. This finding was supported by documenting a physical

interaction between ERCC1/XPF and subunits of the TFIID complex (Kamileri *et al*. 2012b). The unexpected involvement of specific NER factors, apart from TFIIH, in transcriptional regulation was also reported in two additional studies, where the authors independently showed that these factors are important for transcriptional activation of retinoic acid-responsive genes upon cellular stimulation and that a XPC-containing complex acts as an Oct4/Sox2 co-activator to facilitate Nanog expression and pluripotency in embryonic stem cells (Le May *et al*. 2010; Fong *et al*. 2011). These recent observations suggest that NER factors function outside their canonical mode, DNA repair, to facilitate gene transcription in distinct instances (Kamileri *et al*. 2012; Fong *et al*. 2013).

Aim of the study

White adipose tissue is a metabolically active organ, highly responsive to insulin that mainly serves as an energy storage depot by accumulating triacylglycerols, an inert form of lipids (Gesta *et al*. 2007). Lipids are stored in adipocytes, the most abundant cell type of the tissue. In rodents, white adipocytes are of mesenchymal origin and differentiate postnatally into fully functional cells (Han *et al*. 2011), when a transcriptional cascade co-ordinated by the master regulator Peroxisome Proliferator-Activated Receptor γ (PPARγ) is activated in pre-adipocytes (Rosen and MacDougald, 2006). It is apparent that adipose tissue stores energy in a very efficient way. Hence, it becomes a central organ in regulating whole-body energy balance together with other organs, such as the liver, the pancreas and the brain. To do so, it produces and secretes hormones, the so called adipokines, which act both in an endocrine and a paracrine manner, mainly on the central and peripheral nervous system (Rosen and Spiegelman, 2006). Pathological conditions

that alter adipose tissue function impinge on metabolic homeostasis, mainly by altering the levels or pattern of hormone production and secretion by the organ. For example, obesity and lipodystrophy are characterized by adipose tissue dysfunction and lead to the manifestation of severe metabolic abnormalities that ultimately result in reduced lifespan (Hotamisligil, 2006; Fiorenza *et al*. 2011). Apart from leptin and adiponectin, which controls appetite and serves as systemic insulin sensitizer, respectively, adipocytes produce and secrete adipokines with a pro-inflammatory function, such as resistin and lipocalin 2 (Ouchi *et al*. 2011). These molecules have been shown to promote insulin resistance in obese rodents (Steppan *et al*. 2001; Wang *et al*. 2007). Additionally, adipocytes from mice that suffer from obesity produce tumour necrosis factor α (TNFα), a well-known pro-inflammatory cytokine (Hotamisligil *et al*. 1993). Its action has been shown to inhibit insulin receptor signalling in the adipocyte (Hotamisligil *et al*. 1994). On the other hand, lipodystrophic mouse models have also been observed to express pro-inflammatory molecules either in their adipose tissue or systemically. However, their primary cellular source was not identified (Kim *et al*. 2007; Herrero *et al*. 2010). Besides obesity and lipodystrophy, adipose tissue also becomes dysfunctional during ageing (Tchkonia *et al*. 2010). In aged tissues and depending on the depot, pre-adipocytes lose their differentiation ability and acquire a more pro-inflammatory, senescent-like phenotype that affects whole-tissue function (Karagiannides *et al*. 2001; Karagiannides *et al*. 2006; Tchkonia *et al*. 2007).

Although a senescent progenitor pool that drives age-related tissue dysfunction seems plausible, compromised mature adipocytes would also contribute to tissue ageing. Stochastic macromolecular damage accumulation, irrespective of the differentiation stage, could underlie age-related adipose tissue dysfunction (Kirkwood, 2006). In the present

study, we aim to delineate the impact of genomic instability in age-related adipose tissue pathology. To this end, we have employed a tissue-specific DNA repair defective *Ercc1*$^{-/-}$ mouse model that manifests a dramatic loss of adipose tissue.

Results

Loss of adipose tissue in (aP2-*Cre*) *Ercc1*$^{-/-}$ animals

Besides dwarfism, Cockayne Syndrome, Trichothiodystrophy and XPF-ERCC1 deficient patients are characterized by progeroid features, such as cachexia and loss of subcutaneous fat (Schumacher *et al*. 2008). Adipose tissue loss is also observed in normal aging (Sepe *et al*. 2011). To gain greater understanding into the role of unrepaired DNA damage relative to adipose tissue loss of these syndromes, we used the *Ercc1*$^{-/-}$ mouse model which closely mimics both the developmental and the progeroid features seen in XFE patients (Niedernhofer *et al*. 2006). Beginning postnatal day 5 (P5), *Ercc1*$^{-/-}$ animals fail to gain weight and display gradual reduction in epididymal, interscapular and subcutaneous white adipose tissue (WAT) depots. P15 *Ercc1*$^{-/-}$mice show a ~50% decrease in epididymal WAT and a small -albeit not significant- reduction of brown adipose tissue (BAT, **Figure 2A**, **B**).

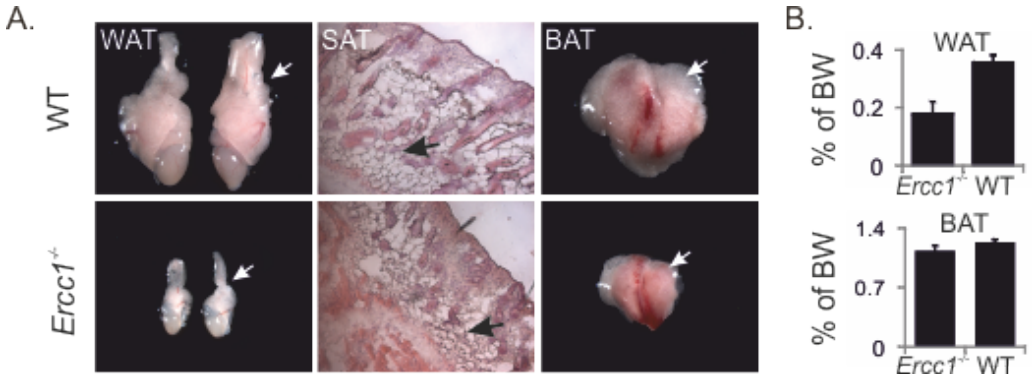

Figure 2 Adipose tissue loss in the *Ercc1*$^{-/-}$ mouse model. (A). Photographs of epididymal, subcutaneous and brown adipose tissue depots of 15 days old WT (upper panels) and *Ercc1*$^{-/-}$ (lower panels) mice. (B). Weight of epididymal white adipose tissue (WAT) and brown adipose tissue (BAT) depots shown as % of body weight (BW) of 15 days old mice. Error bars indicate S.E.M.

Although these mice represent a valid model for XFE syndrome, the complex nature of their phenotype, including developmental abnormalities, progeroid symptoms in several

organs and premature death before reaching sexual maturity, does not allow the comprehensive study of a specific feature. To test whether adipose tissue loss in *Ercc1*$^{-/-}$ mice is the consequence of defects in other organs or is cell-autonomous, we sought to generate tissue-specific *Ercc1*$^{-/-}$ mice by intercrossing animals homozygous for the floxed *Ercc1* allele (*Ercc1*$^{F/F}$) (Verhagen-Oldenampsen et al., 2012) with those carrying the

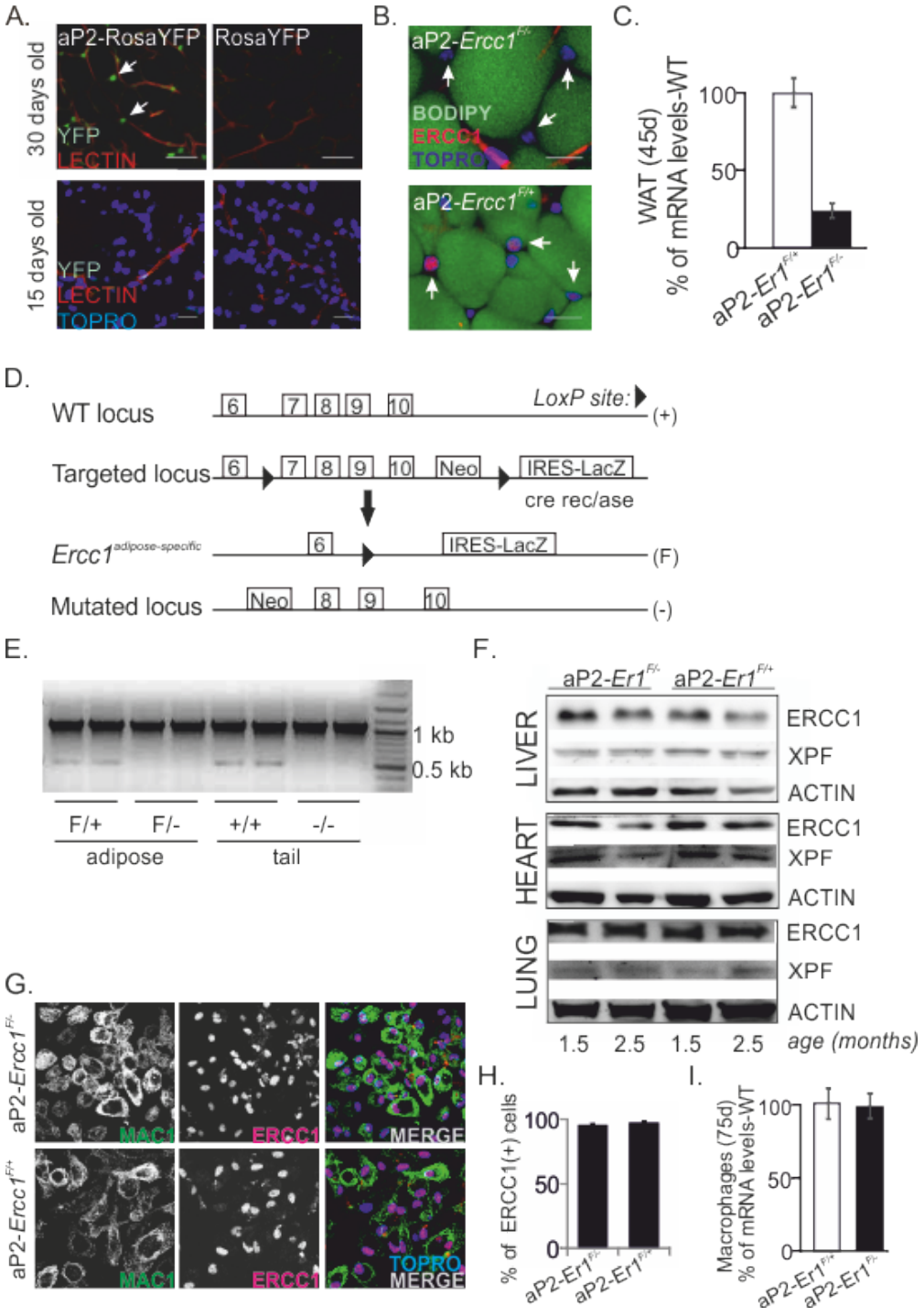

Figure 3 Generation of the adipose tissue-specific *Ercc1*$^{-/-}$ mouse.

adipose protein 2 (aP2)-*Cre* transgene in an *Ercc1* heterozygous background (aP2-*Cre*;*Ercc1*$^{+/-}$ mice); aP2 is a carrier protein for fatty acids that is primarily expressed in adipocytes (Jones *et al*. 2005). Crossing the aP2-*Cre* with Rosa YFP$^{st/st}$ transgenic animals confirmed the specificity of aP2-driven YFP expression to adipocytes at P30 but not at P15 (**Figure 3A**). The cell type-specific ablation of *Ercc1* was already evident in 1.5 months old aP2-*Ercc1*$^{F/-}$ WAT depots, both at the protein and at the mRNA level (**Figure 3B, C**). Excision of the floxed *Ercc1* allele was further confirmed by genomic PCR amplification on DNA derived from aP2-*Ercc1*$^{F/+}$ and aP2-*Ercc1*$^{F/-}$ adipose tissues (**Figure 3D, E**). ERCC1 expression levels in aP2-*Ercc1*$^{F/-}$ organs and cells other than adipocytes remained normal (**Figure 3F-I**). aP2-*Ercc1*$^{F/-}$ mice were born at the expected Mendelian frequency and showed no developmental defects or other pathological features, including any visible defects in adipose tissue; the mRNA levels of *Fabp4* and

Figure 3 Generation of the adipose tissue-specific *Ercc1*$^{-/-}$ mouse. (A). Confocal imaging of aP2-driven YFP expression in adipocytes of 30 days old ROSA-YFP mice. (B). Confocal imaging of aP2-driven Ercc1 ablation in 1.5 months old aP2-*Ercc1*$^{F/-}$ WAT depots. (C). Quantitative (q)PCR mRNA levels of Ercc1 expression in 1.5 months old aP2-*Ercc1*$^{F/-}$ WAT depots. (D). Schematic representation of the targeted *Ercc1* locus. The 3' arm of the wild type (+) *Ercc1* allele consisting of 5 exons (exons 6-10) was targeted to generate the conditional knock-out allele. LoxP sites were inserted 5' to exon 7 and 3' to exon 10, including a Neomycin positive selection cassette (Neo). An IRES-LacZ cassette was added 3' to the second LoxP site. Adipose-specific cre-mediated recombination results in a floxed (F) *Ercc1* allele that lacks exons 7-10. The mutated (-) *Ercc1* allele was generated by substituting exon 7 with a Neo cassette and results in the excision of the *Ercc1* gene. (E). PCR detection of the excised (0.5 kb) Ercc1 allele on adipose genomic DNA (left) from aP2-*Ercc1*$^{F/+}$ and aP2-*Ercc1*$^{F/-}$ mice. Tail genomic DNA (right) from wt and full *Ercc1*$^{-/-}$ mice was used as a control indicating that the primer set does not amplify the mutated *Ercc1* allele. Loading control: corresponding 1 kb band representing the Ercc1 3' utr region that is not deleted upon *Cre* recombination. (F). Western blots of ERCC1 and XPF in liver, heart and lung of 1.5 and 2.5 months old aP2-*Ercc1*$^{F/-}$ and aP2-*Ercc1*$^{F/+}$ mice. (G). Immunofluorescence detection of ERCC1 in isolated peritoneal macrophages of 2.5 months old aP2-*Ercc1*$^{F/-}$ and aP2-*Ercc1*$^{F/+}$ mice. (H). Quantification of ERCC1-positive cells expressed as % of total number of cells per optical field. (I). qPCR mRNA levels of Ercc1 expression in isolated peritoneal macrophages of 2.5 months old aP2-*Ercc1*$^{F/-}$ and aP2-*Ercc1*$^{F/+}$ mice. Error bars indicate S.E.M.

Adiponectin, an adipocyte-secreted hormone previously linked to insulin resistance and diabetes (Kadowaki *et al*. 2006), were comparable between 1.5 months old aP2-*Ercc1*$^{F/-}$ WAT tissues and control animals (**Figure 4A**). Beginning at 2.5 months, aP2-*Ercc1*$^{F/-}$ animals show a slow but steady loss of epididymal, interscapular and subcutaneous fat depots (**Figure 4B**) resulting in a ~30% reduction in body weight (**Figure 4C)**,

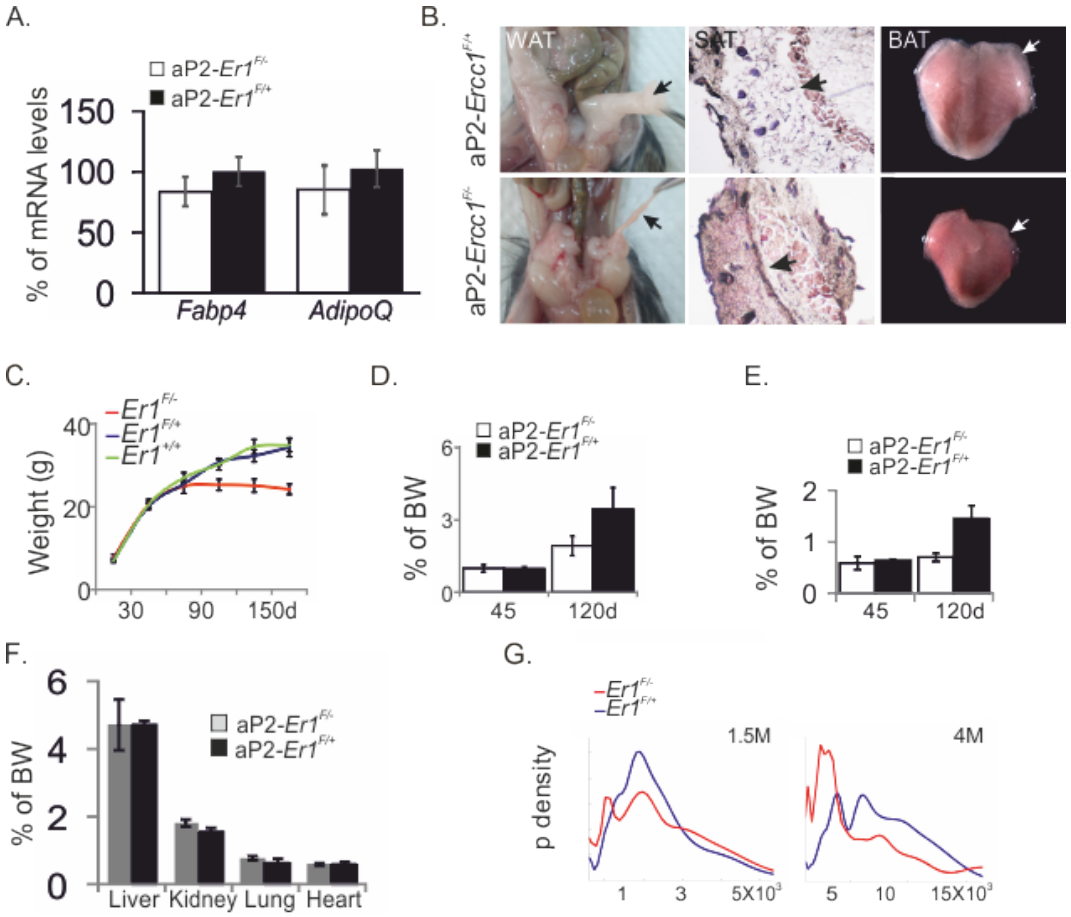

Figure 4 Adipose tissue loss in the aP2-*Ercc1*$^{F/-}$ mouse model. (A). Quantitative (q) PCR mRNA levels of *Fabp4* and *Adipoq* genes in 1.5 months old aP2-*Ercc1*$^{F/-}$ and aP2-*Ercc1*$^{F/+}$ white adipose tissues (WAT). (B). Photographs of epididymal, subcutaneous and brown adipose tissue depots of 4 months old aP2-*Ercc1*$^{F/+}$ (upper panel) and aP2-*Ercc1*$^{F/-}$ (lower panel) mice. (C). Total body weight (in grams) of aP2-*Ercc1*$^{F/-}$ (*Er*$^{F/-}$), aP2-*Ercc1*$^{F/+}$ (*Er*$^{F/+}$) and WT (*Er*$^{+/+}$) mice across 150 days post birth. (D). Weight of epididymal WAT expressed as % of body weight (BW) of aP2-*Ercc1*$^{F/-}$ and aP2-*Ercc1*$^{F/+}$ mice at 1.5 and 4 months of age. (E). Weight of brown adipose tissue (BAT) expressed as % of body weight (BW) of aP2-*Ercc1*$^{F/-}$ and aP2-*Ercc1*$^{F/+}$ mice at 1.5 and 4 months of age. (F). Weights of liver, kidney, lung and heart organs expressed as % of body weight of 4 months old aP2-*Ercc1*$^{F/-}$ and aP2-*Ercc1*$^{F/+}$ mice. (G). Size distribution of adipocytes derived from 1.5 and 4 months old aP2-*Ercc1*$^{F/-}$ (*Er*$^{F/-}$) and aP2-*Ercc1*$^{F/+}$ (*Er*$^{F/+}$) mice. Error bars indicate S.E.M.

a >50% reduction in epididymal WAT (**Figure 4D**) and interscapular BAT depots (**Figure 4E**); the weight of other organs was comparable to that of control animals (**Figure 4F**). Unlike the 1.5 months old aP2-*Ercc1*$^{F/-}$ animals, computer image analysis revealed substantial differences in the size distribution of adipocytes of 4 months old aP2-*Ercc1*$^{F/-}$ animals compared to age-matched controls (**Figure 4G**). Thus, adult mice lacking ERCC1 specifically in the adipose tissue exhibit marked WAT and BAT abnormalities; importantly, both adipose tissue depots develop normally in these mice with defects gradually appearing at later stages in life.

Adipose tissue morphological changes and metabolic abnormalities in aP2-*Ercc1*$^{F/-}$ mice

Scanning electron microscopy of epididymal WAT and BAT derived from 15 days old *Ercc1*$^{-/-}$ and wt animals revealed no apparent differences (**Figure 5A**). Both *Ercc1*$^{-/-}$ and wt adipose depots, show areas of dense cilia formation characteristic of adipogenic differentiation during development (Satir *et al*. 2010) (**Figure 5A**; embedded magnification). Likewise, the 1.5 months old aP2-*Ercc1*$^{F/-}$ and aP2-*Ercc1*$^{F/+}$ white adipocytes appeared healthy with spherical and unilocular lipid depots (**Figure 5B**). In contrast, the WAT of 4 months old aP2-*Ercc1*$^{F/-}$ animals showed areas of ruptured basal membrane (**Figure 5C-i**) and frequent loss of adipocytes (**Figure 5C-ii**); red blood cells were sporadically found to occupy empty adipocyte cavities, likely marking the former presence of adipocyte-associated capillaries (**Figure 5C-ii**; embedded magnification). Staining with Platelet/Endothelial Cell Adhesion Molecule 1 (PECAM-1) revealed a dense and well-structured vasculature in aP2-*Ercc1*$^{F/-}$ WAT samples compared to controls (**Figure 5F**). We also found areas of ciliae recurrence (**Figure 5C-iii**; embedded magnification) and extensive interstitial tissue deposition marking fibrosis at sites of tissue damage both in WAT and in BAT of 4 months old aP2-*Ercc1*$^{F/-}$ animals (**Figure 5C-iv and 5E**). None of these pathological features were observed in the 4 months old aP2-*Ercc1*$^{F/+}$ WAT or BAT depots (**Figure 5D, E**).

These degenerative features of adipose tissue, also seen in lipodystrophic mice, prompted us to further characterize the metabolic profile of the aP2-*Ercc1*$^{F/-}$ animals. Due to the progressive nature of the phenotype, we focused our studies on 4 months old mice. Serum cholesterol levels were normal in 4 months old aP2-*Ercc1*$^{F/-}$ mice and triglycerides were elevated (**Figure 6A**). Serum and white adipose tissue (WAT) adiponectin levels

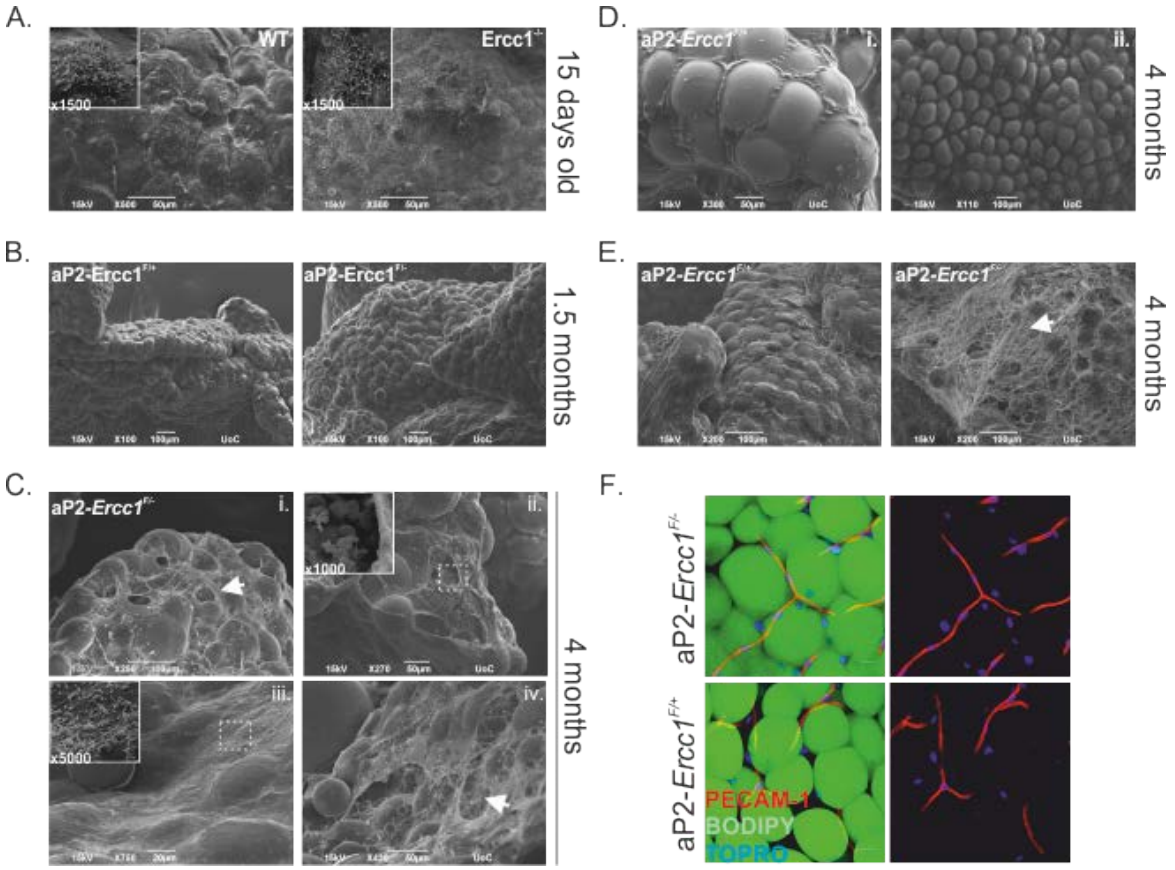

Figure 5 Progressive adipose tissue degeneration in aP2-*Ercc1*$^{F/-}$ mice. (A). Scanning electron micrographs (SEM) of 15 days old WT and *Ercc1*$^{-/-}$ white adipose tissue (WAT) depots. Insert: higher magnification showing ciliae in both tissues. (B). SEM of 1.5 months old aP2-*Ercc1*$^{F/+}$ and aP2-*Ercc1*$^{F/-}$ WAT depots. (C). SEM of 4 months old aP2-*Ercc1*$^{F/-}$ WAT depots showing: i. basement membrane rupture, ii. Adipocyte depletion (insert: higher magnification indicating capillary rupture), iii. ciliae recurrence (insert: higher magnification of ciliae), iv. fibrosis. (D). SEM of 4 months old aP2-*Ercc1*$^{F/+}$ WAT depots. (E). SEM of 4 months old aP2-*Ercc1*$^{F/+}$ and aP2-*Ercc1*$^{F/-}$ BAT depots. (F). Confocal imaging of 4 months old aP2-*Ercc1*$^{F/-}$ and aP2-*Ercc1*$^{F/+}$ WAT depots showing normal vascular endothelium with anti-PECAM-1 staining.

were reduced compared to littermate controls (**Figure 6B, J**). Prior to glucose and insulin tolerance tests, 4 months old aP2-*Ercc1*$^{F/-}$ animals had basal plasma glucose levels comparable to wild-type mice after a 5 hour fast (**Figure 6C, D**). Upon intraperitoneal glucose infusion, the 4 months old aP2-*Ercc1*$^{F/-}$ mice had increased plasma glucose levels compared to controls (**Figure 6C**). However, aP2-*Ercc1*$^{F/-}$ and aP2-*Ercc1*$^{F/+}$ animals had comparable serum glucose levels following intraperitoneal insulin infusion (**Figure 6D**).

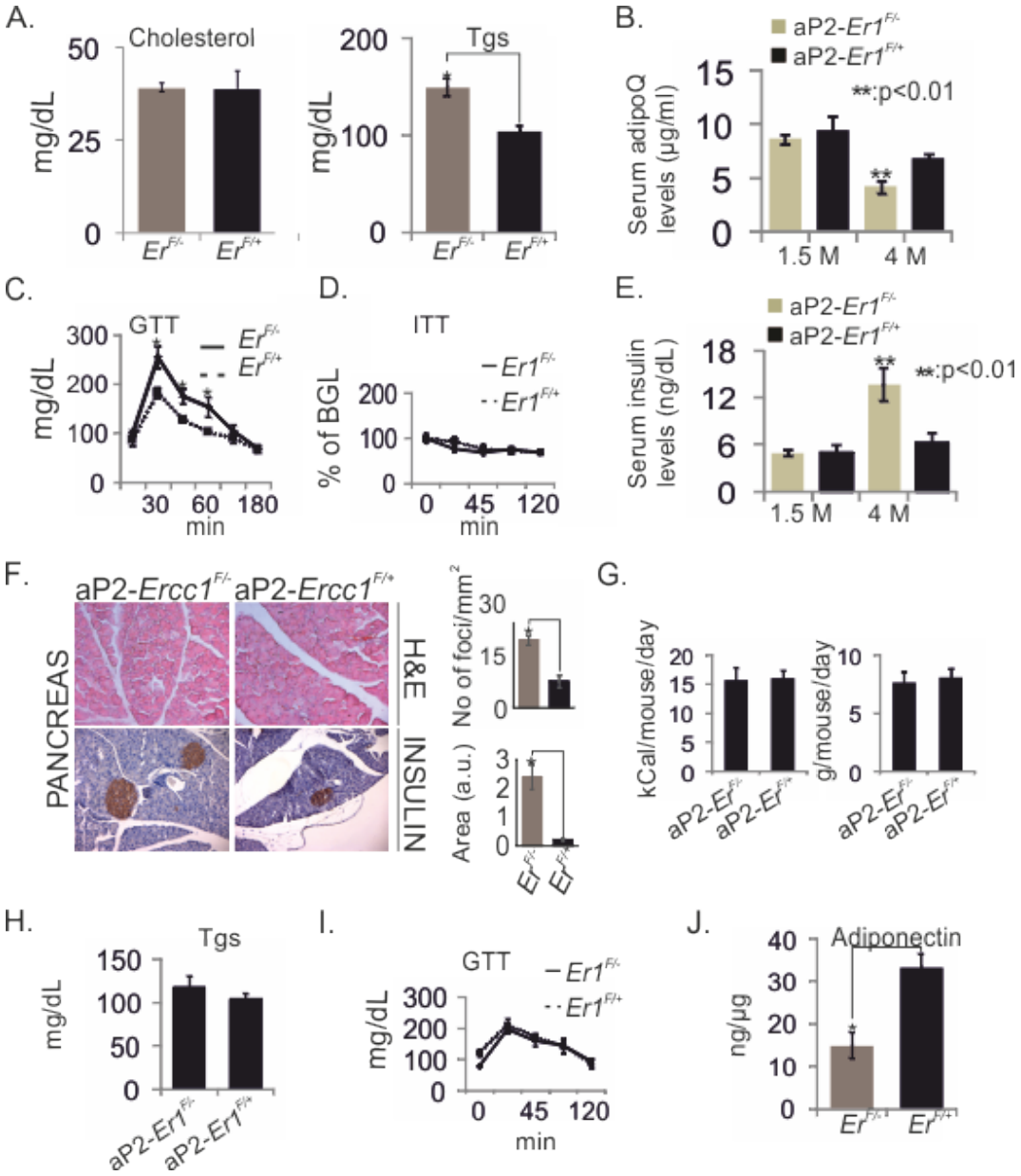

Figure 6 Metabolic abnormalities in the lipodystrophic aP2-*Ercc1*$^{F/-}$ mice. (A). Serum cholesterol and triglycerides levels in 4 months old aP2-*Ercc1*$^{F/-}$ (*Er*$^{F/-}$) and aP2-*Ercc1*$^{F/+}$ (*Er*$^{F/+}$) mice. (B). Serum adiponectin protein levels in 1.5 and 4 months old aP2-*Ercc1*$^{F/-}$ and aP2-*Ercc1*$^{F/+}$ mice. (C). Glucose tolerance test in 4 months old aP2-*Ercc1*$^{F/-}$ (*Er*$^{F/-}$) and aP2-*Ercc1*$^{F/+}$ (*Er*$^{F/+}$) mice. (D). Insulin tolerance test in 4 months old aP2-*Ercc1*$^{F/-}$ (*Er*$^{F/-}$) and aP2-*Ercc1*$^{F/+}$ (*Er*$^{F/+}$) mice. Plasma glucose after infusion is indicated as % of basal plasma glucose levels (BGL). (E). Serum insulin levels in 1.5 and 4 months old aP2-*Ercc1*$^{F/-}$ and aP2-*Ercc1*$^{F/+}$ mice. (F). Hematoxylin-Eosin (H&E, upper panels) and insulin (lower panels) staining of 4 months old aP2-*Ercc1*$^{F/-}$ and aP2-*Ercc1*$^{F/+}$ pancreata. Estimates of number per mm^2 and area of insulin producing islets are shown in graphs. (G). Food and water intake (as indicated) of 2.5 months old aP2-*Ercc1*$^{F/-}$ and aP2-*Ercc1*$^{F/+}$ mice. (H). Serum triglycerides levels in 1.5 months old aP2-*Ercc1*$^{F/-}$ and aP2-*Ercc1*$^{F/+}$ mice. (I). Glucose tolerance test in 1.5 months old aP2-*Ercc1*$^{F/-}$ (*Er*$^{F/-}$) and aP2-*Ercc1*$^{F/+}$ (*Er*$^{F/+}$) mice. (J). White adipose tissue adiponectin protein levels in 4 months old aP2-*Ercc1*$^{F/-}$ (*Er*$^{F/-}$) and aP2-*Ercc1*$^{F/+}$ (*Er*$^{F/+}$) mice. Error bars indicate S.E.M., * p-value≤0.05, ** p-value≤0.01.

Basal serum insulin levels and staining of pancreata from fasted aP2-*Ercc1*$^{F/-}$ mice revealed hyperinsulinaemia followed by increased number and size of insulin producing foci compared to aP2-*Ercc1*$^{F/+}$ controls (**Figure 6E, F**). Food and water intake measurements in 2.5 month old aP2-*Ercc1*$^{F/-}$ and aP2-*Ercc1*$^{F/+}$ animals over a period of 30 days revealed no significant differences (**Figure 6G**). None of the abovementioned metabolic abnormalities were observed in 1.5 months old aP2-*Ercc1*$^{F/-}$ mice (**Figure 6B, E, H, I**), further supporting the progressive nature of aP2-*Ercc1*$^{F/-}$ lipodystrophic phenotype. Oil Red O staining of 4 months old aP2-*Ercc1*$^{F/-}$ visceral organs revealed accumulation of triglycerides in heart and muscle, but not in liver, kidney or spleen (**Figure 7A**).

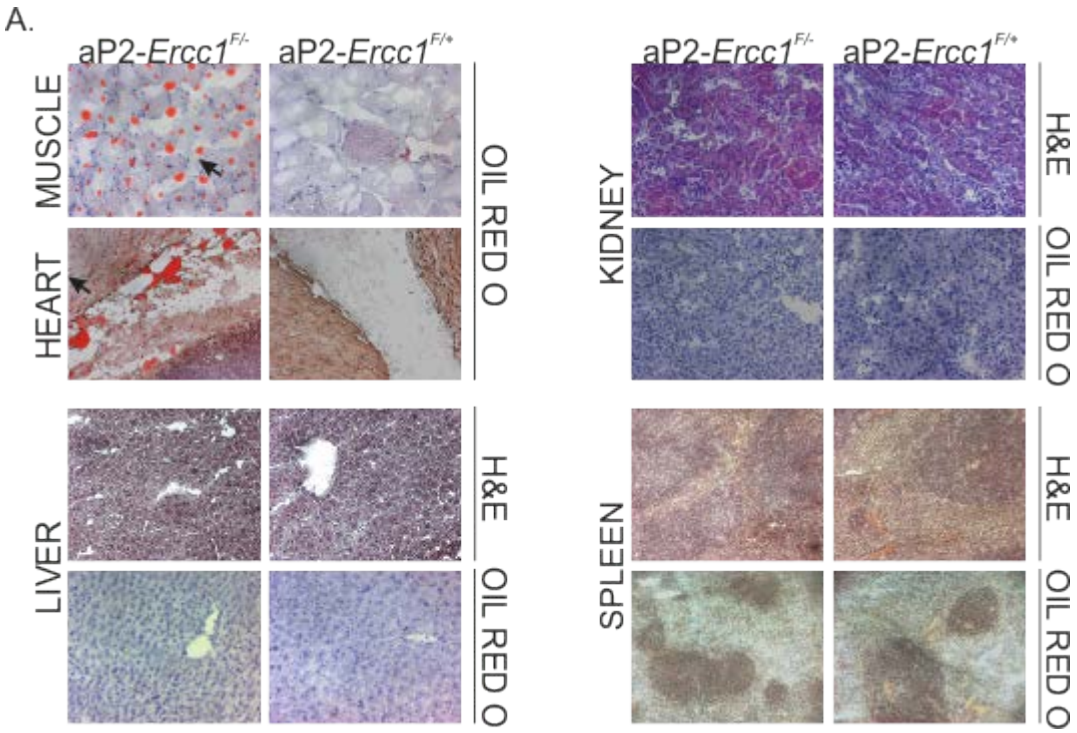

Figure 7 Ectopic lipids accumulation in lipodystrophic aP2-*Ercc1*$^{F/-}$ mice. (A). Histological examination (H&E – hematoxylin and eosin) and Oil Red O staining of visceral organs of 4 months old aP2-*Ercc1*$^{F/-}$ and aP2-*Ercc1*$^{F/+}$ mice.

Thus, similar to other lipodystrophic animal models, the aP2-*Ercc1*$^{F/-}$ animals exhibit metabolic abnormalities that are associated with type II diabetes mellitus. Together, these findings resemble the pathological abnormalities seen in progressive lipodystrophies ultimately leading to severe metabolic dysfunction (Hegele *et al*. 2007).

Transcriptome analysis of epididymal WAT depots in *Ercc1*$^{-/-}$ animals

To further elucidate the role of ERCC1 in white adipose tissue (WAT) we scanned the transcriptome of 15 days old wt and *Ercc1*$^{-/-}$ epididymal WAT (n=4). Two-way analysis of variance of Affymetrix mouse genome arrays revealed 2254 genes with significantly changed expression patterns between the *Ercc1*$^{-/-}$ and wt fat depots ($p \leq 0.05$, $\geq \pm 1.2$ fold change, **Table S1**). Using the set of 2254 genes, we identified those GO-classified biological processes with a significantly disproportionate number of responsive genes relative to those printed on microarrays (false detection rate ≤ 0.01). This approach revealed five biological processes including the response to DNA interstrand crosslinks (ICLs) and double-strand breaks (DSBs), pro-inflammatory signaling, nuclear receptor and growth factor signaling as well as a response to oxidative and other stress (**Figure 8A**). These transcriptional changes could represent genuine changes in gene regulation as well as reflect a decrease in the fraction of adipocytes relative to stromal cells in *Ercc1*$^{-/-}$

A.

Overrepresented Pathways

	p	R
Response to DNA DSBs		
ATM Signaling	3.75	0.30
Response to DSBs by HR	3.65	0.28
G2/M DNA Damage Checkpoint	2.33	0.25
Proinflammatory signaling		
TNF receptor Signaling	2.89	0.24
Interleukin Signaling	2.44	0.20
NF-kappa B Signaling	2.14	0.18
nNOS Signaling	1.53	0.16
Nuclear Receptor signaling		
PPAR Signaling	2.00	0.19
RAR Activation	1.68	0.16
Transcr/nal Repression Signaling	1.53	0.26
Growth factor signaling		
mTOR Signaling	4.72	0.21
EGF Signaling	2.53	0.25
PI3K/AKT Signaling	2.20	0.17
Insulin Receptor Signaling	2.12	0.18
Response to Stress		
HMGB1 Signaling	3.53	0.24
NRF2 Oxidative Stress Response	2.93	0.19

Figure 8 Overrepresented pathways in *Ercc1*$^{-/-}$ white adipose tissue. (A). Overrepresented biological processes in 15 days old *Ercc1*$^{-/-}$ WAT depots as compared to age-matched WT mice. p: -log of p-value, calculated by Fischer's exact test (right-tailed); *R*: ratio of number of genes in the indicated pathway divided by the total number of genes that make up that pathway.

WAT depots. *Pparγ*$^{ldi/+}$ animals carry a targeted allele that confers conditional dominant lipodystrophy in mice (Kim *et al*. 2007). We, therefore, compared the gene expression profiles of 10-week old *Pparγ*$^{ldi/+}$ and P15 *Ercc1*$^{-/-}$ gonadal fat pads. Despite the big difference in age between the two different animal models, we found 768 genes that changed significantly in WAT of both *Pparγ*$^{ldi/+}$ and *Ercc1*$^{-/-}$ mice relative to their wt counterparts. This reflects 34% of the significantly altered genes in *Ercc1*$^{-/-}$ WAT compared to wt mice. Of these, 456 genes (20%) in *Pparγ*$^{ldi/+}$ gonadal fat depots also shared the same direction in expression (**Figure 9A; Table S2**). Interestingly, we find that

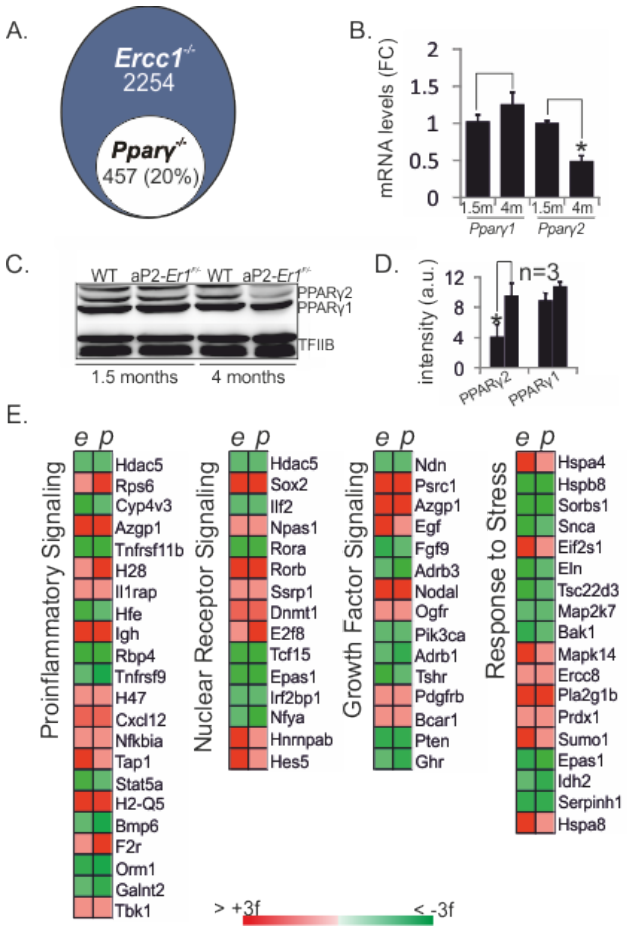

Figure 9 Lipodystrophic gene expression signature in *Ercc1*$^{-/-}$ adipose tissue. (A). Venn diagram representing genes with shared expression changes between *Pparγ*$^{ldy/+}$ and *Ercc1*$^{-/-}$ white adipose tissue (WAT). (B). Quantitative (q) PCR mRNA levels of *Pparγ1* and *Pparγ2* genes in 1.5 and 4 months old aP2-*Ercc1*$^{F/-}$ WAT as compared to control mice. (C, D). Western blot (C) and quantification (D, average intensity in arbitrary units, a.u.) of PPARγ1/2 protein levels in 4 months old aP2-*Ercc1*$^{F/-}$ and aP2-*Ercc1*$^{F/+}$ WAT. (E).Heatmap representation of significant gene expression changes between *Ercc1*$^{-/-}$ (*e*) and *Pparγ*$^{ldy/+}$ (*p*) WAT depots. Error bars represent S.E.M., * p-value≤0.05.

PPARγ2, but not PPARγ1 protein and mRNA levels are reduced in the 4 months old aP2-*Ercc1*$^{F/-}$ animals (**Figure 9B-D**). With the exception of the response to DNA ICLs/DSBs which was seen exclusively in *Ercc1*$^{-/-}$ mice, the set of 456 genes also found in *Pparγ*$^{ldi/+}$ fat depots was associated with the same over-represented biological themes identified in *Ercc1*$^{-/-}$ fat pads (**Figure 9E**). Quantitative (q) PCR and protein immunofluorescence analysis confirmed the validity of these results (**Figure 10A, B**) in the aP2-*Ercc1*$^{F/-}$ mouse as well. Taken together, these findings reveal that a lipodystrophic gene expression signature is established early in the fat of *Ercc1*$^{-/-}$ progeroid mice.

A defect in *Ercc1*$^{-/-}$ WAT depots triggers accumulation of γ-H2AX, RAD51 and FANCI foci in aP2-*Ercc1*$^{F/-}$ gonadal fat pads

During NER, XPF-ERCC1 makes a single-strand nick near the lesion, which is critical for excision of the damage and thought to play an analogous role in DNA ICL repair (Niedernhofer *et al*. 2004). In line with the up-regulation of genes associated with the repair of DNA ICLs and DSBs in 15 days old *Ercc1*$^{-/-}$ WAT depots, several genes associated with the repair of DNA ICLs and DSBs showed increased mRNA levels in 4 months old but not in the 1.5 months old aP2-*Ercc1*$^{F/-}$ WAT depots (**Figure 10A**).

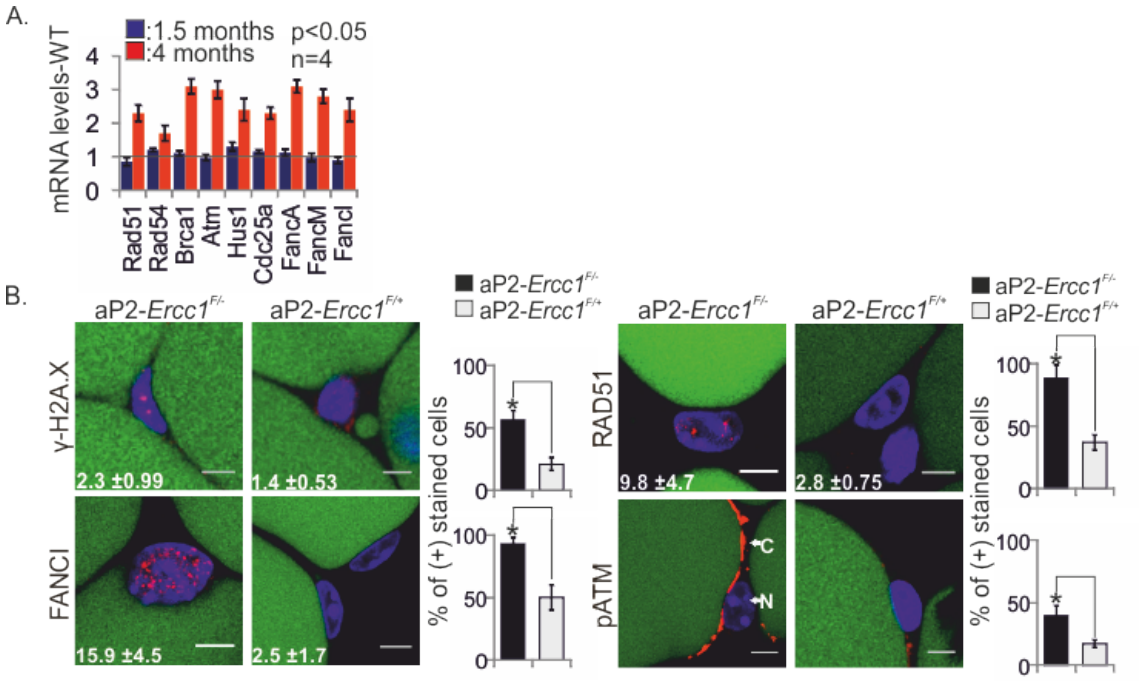

Figure 10 DNA damage response in aP2-*Ercc1*$^{F/-}$ WAT depots. (A). Quantitative (q) PCR mRNA levels of genes associated with a response to DNA ICLs and DSBs in 1.5 and 4 months old aP2-*Ercc1*$^{F/-}$ white adipose tissue (WAT) depots as compared to controls. Black dotted line: WT mRNA levels. (B). Immunofluorescence detection and quantification of γ-H2A.X, FANCI, RAD51 and phospho-ATM foci in aP2-*Ercc1*$^{F/-}$ and aP2-*Ercc1*$^{F/+}$ WAT depots. Numbers in lower left corner indicate average number of foci per nucleus ± s.e.m. Error bars indicate S.E.M., * p-value≤0.05, N=nucleus, C=cytoplasm, scale bar=5 μm.

Phosphorylated histone H2A.X (γ-H2A.X)-containing foci accumulate at sites of DNA breaks (Fernandez-Capetillo *et al*. 2004). γ-H2A.X staining of aP2-*Ercc1*$^{F/-}$ adipocytes revealed a punctuate pattern of foci; γ-H2A.X gradually accumulated from 1-2

foci/nucleus in the 1.5 months old animals (~20% positive cells; data not shown) to approximately 3 or more foci/nucleus in the 4 months old gonadal fat depots (~56% positive cells; **Figure 10B**). Similarly, RAD51, a protein involved in the repair of DSBs by homologous recombination (HR) (Elliott and Jasin, 2002) and FANCI involved in the repair of DNA inter-strand cross-links (ICLs) (Sato *et al*. 2012) also formed foci that gradually increased from 1-2 foci/nucleus in the 1.5 months old mice to >10 foci/nucleus in 4 months old aP2-*Ercc1*$^{F/-}$ animals (**Figure 10B**). Similar to others, (Yang *et al*. 2011; Yang and Kastan, 2000), we found phosphorylated ATM to be predominantly cytoplasmic in adipocytes of 4 months old aP2-*Ercc1*$^{F/-}$ mice (**Figure 10B**). Staining with Caspase 3 revealed few, if any, apoptotic cells in 1.5 and 4 months old aP2-*Ercc1*$^{F/-}$ gonadal fat pads (data not shown). Instead, staining of non-fixed tissues with TO-PRO-3 revealed a significant increase in necrotic cells (15.4%) in 4 months old aP2-*Ercc1*$^{F/-}$ WAT depots compared to age-matched controls or to 1.5 months old aP2-*Ercc1*$^{F/-}$ animals (**Figure 11A**). Damage-associated molecular pattern (DAMP) molecules are released

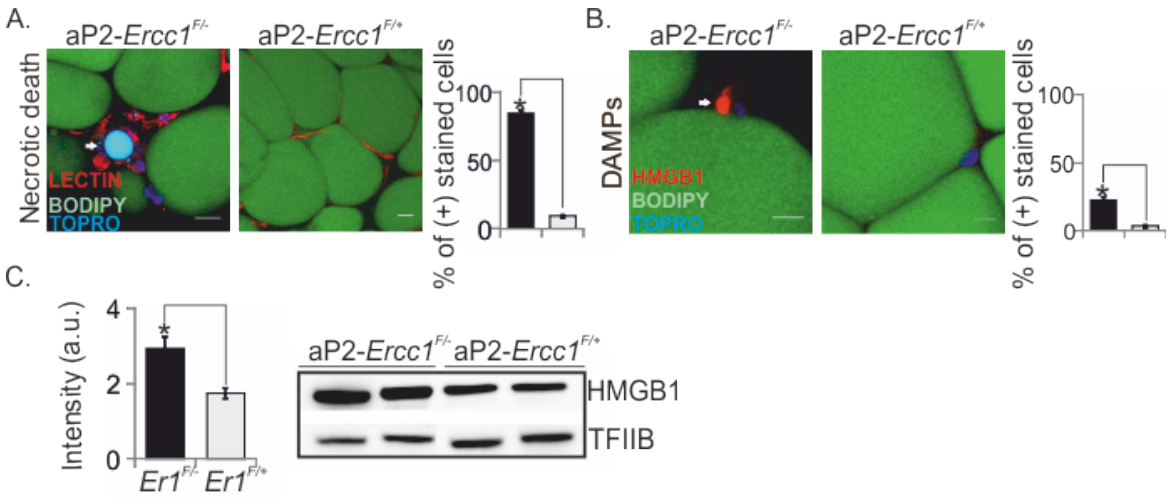

Figure 11 Necrotic death and DAMPs in aP2-*Ercc1*$^{F/-}$ WAT depots. (A, B). Confocal imaging and quantification of 4 months old aP2-*Ercc1*$^{F/-}$ and control white adipose tissue (WAT) depots revealing necrotic death (A) and HMGB1 release (B). (C). Western blot and quantification (average intensity in arbitrary units, a.u.) of HMGB1 protein levels in 4 months old aP2-*Ercc1*$^{F/-}$ (*Er*$^{F/-}$) and control (*Er*$^{F/+}$) WAT depots. Bodipy: lipid droplet, Lectin: endothelia, Topro: necrotic cells/nuclei, scale bar=20 μm, error bars indicate S.E.M., * p-value≤0.05.

by stressed cells undergoing necrosis that act as endogenous danger signals to promote and exacerbate defense responses, including inflammation (Miyake and Yamasaki, 2012). In 4 months old aP2-*Ercc1*$^{F/-}$ WAT, we detected the release of high-mobility group protein B1 (HMGB1), a central mediator of senescent phenotypes (Davalos *et al*. 2013) that is associated with DAMPs and is known to initiate and perpetuate immune responses in the noninfectious inflammatory response at sites of injury (**Figure 11B**) (Miyake and Yamasaki, 2012). HMGB1 protein levels were elevated in 4 months old aP2-*Ercc1*$^{F/-}$ WAT depots compared to those from age-matched wt mice (**Figure 11C**). Thus, tissue-specific ablation of *Ercc1* gene triggers the gradual accumulation of persistent cytotoxic DNA damage, which in turn causes necrotic cell death and the release of DAMPs on the surface of damaged adipocytes *in vivo*.

Persistent DNA damage triggers chronic inflammation in adipose tissue

Adipose tissue, as other metabolic organs, hosts macrophages, namely adipose tissue-resident macrophages (ATMs), which contribute to maintaining organ metabolic homeostasis (Ouchi *et al*. 2011). In non-physiological conditions these cells accumulate in so-called 'crown-like' structures (CLS) surrounding necrotic adipocytes (Sun *et al*. 2011). Unlike the 4 months old wt or the younger 1.5 months aP2-*Ercc1*$^{F/-}$ animals, confocal imaging of whole-mount 4 months old aP2-*Ercc1*$^{F/-}$ WAT revealed the presence of BrdU^{+} cells in CLS (**Figure 12A**) and infiltrating cells expressing macrophage antigens 1 (MAC1^{+}) and 3 (MAC3^{+}) that formed syncytia around dying adipocytes (**Figure 12A**).

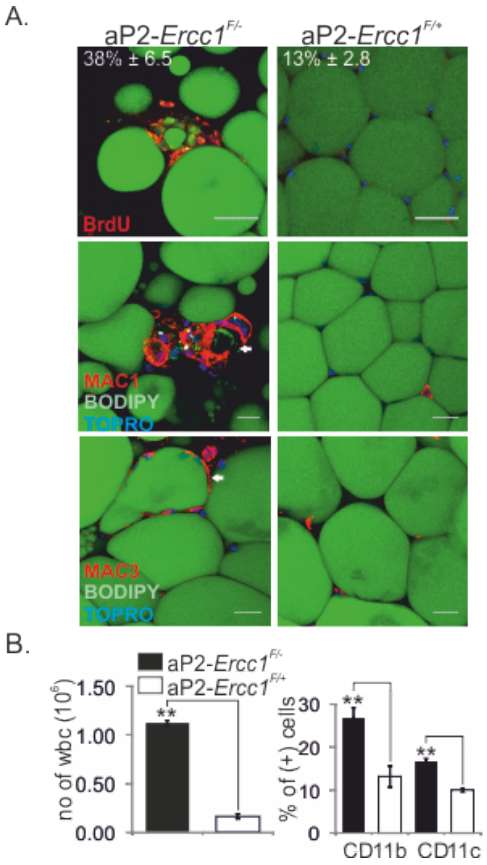

Figure 12 Leukocyte infiltration in the aP2-*Ercc1*$^{F/-}$ WAT depots. (A). Confocal imaging of 4 months old aP2-*Ercc1*$^{F/-}$ and aP2-*Ercc1*$^{F/+}$ white adipose tissue (WAT) depots, marking the presence of BrdU- (upper panels), Mac1- (middle panels) and Mac3-positive (lower panels) infiltrating cells. Upper left numbers indicate average number of positive cells per focal plane ± s.e.m. (B). Number of total white blood cell (WBC) counts (left) and CD11b- or CD11c-positive cells, as determined by FACS (right), in the stromal-vascular fraction of 4 months old aP2-*Ercc1*$^{F/-}$ and aP2-*Ercc1*$^{F/+}$ WAT depots. Bodipy: lipid droplet, Topro: nuclei, error bars indicate S.E.M., ** p-value≤0.01, scale bar=20 μm.

Both proteins are essential for leukocyte activation and MAC3 is a marker of differentiated macrophages (Khazen *et al*. 2005). Leukocyte infiltration of 4 months old aP2-*Ercc1*$^{F/-}$ WAT depots was further confirmed by total white blood cell (WBC) counts and FACS analysis, which revealed a significant increase in the number of WBCs and an increase of CD11b^{+} and CD11c^{+} stained cells in the stromal-vascular fraction, marking the presence of activated macrophages in these animals (**Figure 12B**). MAC1^{+} cells in 4 months old aP2-*Ercc1*$^{F/-}$ fat depots expressed iNOS, a potent inducer of chronic inflammation and a marker of activated macrophages (M1-type), CD45 – a marker of leukocytes and two endothelial adhesion molecules ICAM-1 and VCAM, which are known to facilitate the accumulation of monocytes at sites of tissue injury (**Figure 13A**).

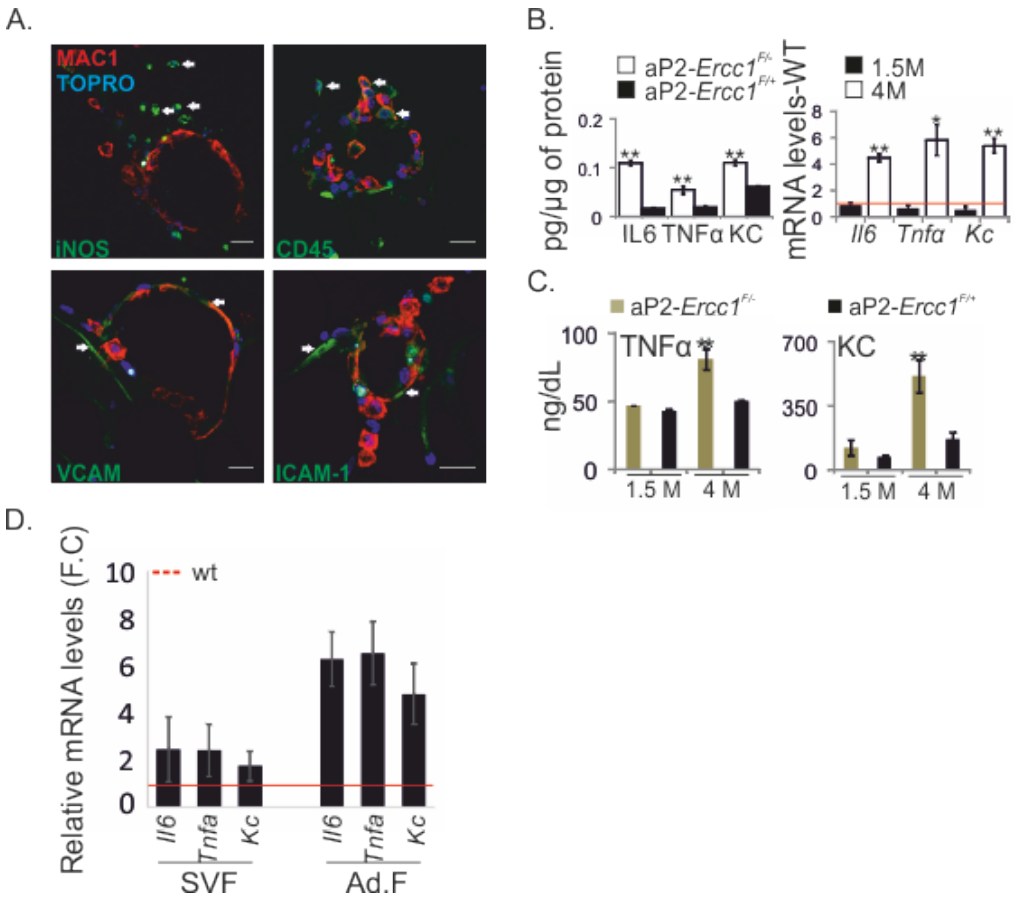

Figure 13 Pro-inflammatory signalling in the aP2-*Ercc1*$^{F/-}$ WAT depots. (A). Confocal imaging of 4 months old aP2-*Ercc1*$^{F/-}$ white adipose tissue (WAT) depots, marking the presence of iNOS, CD45, VCAM and ICAM-1 molecules in the MAC1-enriched crown-like structures. (B). Protein (left) and mRNA (right) levels of pro-inflammatory IL6, TNFα and KC molecules in 4 months old aP2-*Ercc1*$^{F/-}$ and aP2-*Ercc1*$^{F/+}$

ELISA assay on fat tissue revealed elevated IL-6, TNF-α, and KC (murine homologue to IL-8) protein levels in the 4 months old aP2-*Ercc1*$^{F/-}$ WAT depots compared to controls (**Figure 13B**). Similarly, *Il6, Tnfα,* and *Kc* mRNA levels were increased in the adipose tissue of 4 months old aP2-*Ercc1*$^{F/-}$ animals compared to younger mice of the same genotype (**Figure 13B**; as indicated).Circulating TNF-α and KC protein levels were also markedly elevated, as measured in the sera of 4 months old aP2-*Ercc1*$^{F/-}$ animals; IL-6 was undetectable (**Figure 13C**). As activated infiltrating macrophages also express pro-inflammatory cytokines, we further analyzed the expression of *Il6*, *Tnfα*, and *Kc* mRNA levels both in the stromal-vascular and the adipocyte-rich fractions of 4 months old aP2-*Ercc1*$^{F/-}$ and aP2-*Ercc1*$^{F/+}$ WAT depots. Increased expression of pro-inflammatory cytokines was confirmed for the stromal-vascular fraction of aP2-*Ercc1*$^{F/-}$ WAT depots. Importantly, the *Il6*, *Tnfα*, and *Kc* mRNA levels were substantially elevated in the adipocyte-rich fraction of aP2-*Ercc1*$^{F/-}$ WAT depots as compared to aP2-*Ercc1*$^{F/+}$ controls (**Figure 13D**). Similar data were obtained from an additional mouse model, the *Ercc1*$^{\Delta/-}$ animals which carry a seven amino acid carboxyl terminal deletion in *Ercc1* gene (Weeda *et al*. 1997)**.** Nine-week old *Ercc1*$^{\Delta/-}$ animals showed a substantial loss of WAT depots (n=9); we also find increased IL6, TNFα, and KC protein levels in the 9- and 20-week old *Ercc1*$^{\Delta/-}$ WAT depots as well as at the mRNA level of 20-week old *Ercc1*$^{\Delta/-}$ WAT depots relative to control animals (n=4; **Figure 14A-D**).

Figure 13 (WAT) depots. Red dotted line: wt levels. (C). Circulating TNFα and KC protein levels in 1.5 and 4 months old aP2-*Ercc1*$^{F/-}$ and aP2-*Ercc1*$^{F/+}$ sera. (D). Quantitative (q) PCR mRNA levels of *Il6*, *Tnfα* and *Kc* genes in the stromal-vascular (SVF) and adipocyte-rich (Ad.F) fractions of 4 months old aP2-*Ercc1*$^{F/-}$ WAT. Red dotted line: wt levels. Topro: nuclei, error bars indicate S.E.M., * p-value≤0.05, ** p-value≤0.01, scale bar=20 μm.

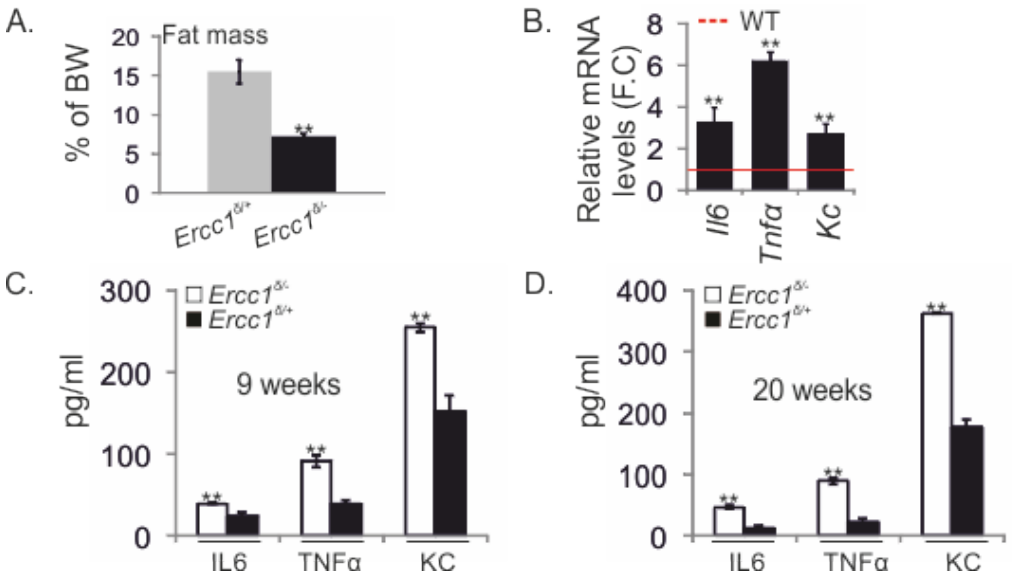

Figure 14 Adipose tissue loss and pro-inflammatory signalling in the *Ercc1*$^{\Delta/-}$ mouse model. (A). Weight of white adipose tissue (WAT) depots of 9-week old *Ercc1*$^{\Delta/+}$ and *Ercc1*$^{\Delta/-}$ mice shown as % of body weight (BW). (B). Quantitative (q) PCR mRNA levels of *Il6*, *Tnfα* and *Kc* genes in WAT of 20-week old *Ercc1*$^{\Delta/-}$ mice. Red dotted line: wt levels. (C, D). IL6, TNFα and KC protein levels of 9-week (C) and 20-week (D) old *Ercc1*$^{\Delta/-}$ and *Ercc1*$^{\Delta/+}$ WAT depots. Error bars indicate S.E.M., ** p-value≤0.01.

Together, our findings show that the formation of DNA damage foci correlates with the onset of pro-inflammatory signals in aP2-*Ercc1*$^{F/-}$ fat depots; the pro-inflammatory response is cell-autonomous as it is initiated by adipocytes rather than by infiltrating macrophages to necrotic adipocytes. The latter possibly contribute to the onset of a systemic pro-inflammatory response and the accompanied metabolic abnormalities observed in 4 months old aP2-*Ercc1*$^{F/-}$ mice.

ICLs induce a pro-inflammatory response in adipocytes

Next, we sought to investigate whether DNA damage directly contributes to pro-inflammatory cytokine production in adipocytes. To this end, we used an *ex vivo* adipogenesis assay in which naive primary wt and *Ercc1*$^{-/-}$ embryonic fibroblasts (MEFs) were exposed to an adipogenic stimulus for 13 days. This led to *de novo* lipid accumulation marking the differentiated, functional adipocytes expressing adipocyte-specific markers, including *Cebpα*, *Fabp4*, *Adiponectin* and *Adipsin* genes (**Figure 15A**). Unlike the wt adipocytes or undifferentiated *Ercc1*$^{-/-}$ MEFs, *Ercc1*$^{-/-}$ adipocytes showed a dramatic accumulation of spontaneous γ-H2AX, pATM and FANCI, but not RAD51 foci (**Figure 15B**). In addition, *Ercc1*$^{-/-}$ adipocytes showed increased *Tnfα*, *Il6* and *Kc* mRNA levels compared to wt adipocytes when compared to corresponding undifferentiated controls (**Figure 15C; as indicated**). Thus, irreparable DNA lesions in otherwise unchallenged *Ercc1*$^{-/-}$ adipocytes trigger the production of pro-inflammatory factors. To further test this, we treated wt adipocytes with mitomycin C (MMC), a potent inducer of DNA cross-links. This led to an increase in *Tnfα*, *Il6* and *Kc* mRNA levels (**Figure 15C; as indicated**); similar to our previous findings, the increase in pro-inflammatory cytokine mRNA levels was substantially higher in MMC-treated adipocytes than MEFs relative to corresponding untreated controls. As the aP2 promoter selected in our work has been reported to be expressed also in macrophages (Mao *et al*. 2009), we tested whether *Ercc1* expression is compromised in macrophages at the origin of the phenotype observed in aP2-*Ercc1*$^{F/-}$ WAT depots. We found *Ercc1* levels in macrophages to be comparable at both the mRNA and the protein levels in 2.5 months old aP2-*Ercc1*$^{F/-}$ compared to aP2-*Ercc1*$^{F/+}$ animals (**Figure 3G-I**). Taken together, our findings suggest that the up-regulation of pro-inflammatory genes is cell autonomous; it requires the presence of persistent DNA damage foci and is exacerbated in adipocytes compared to

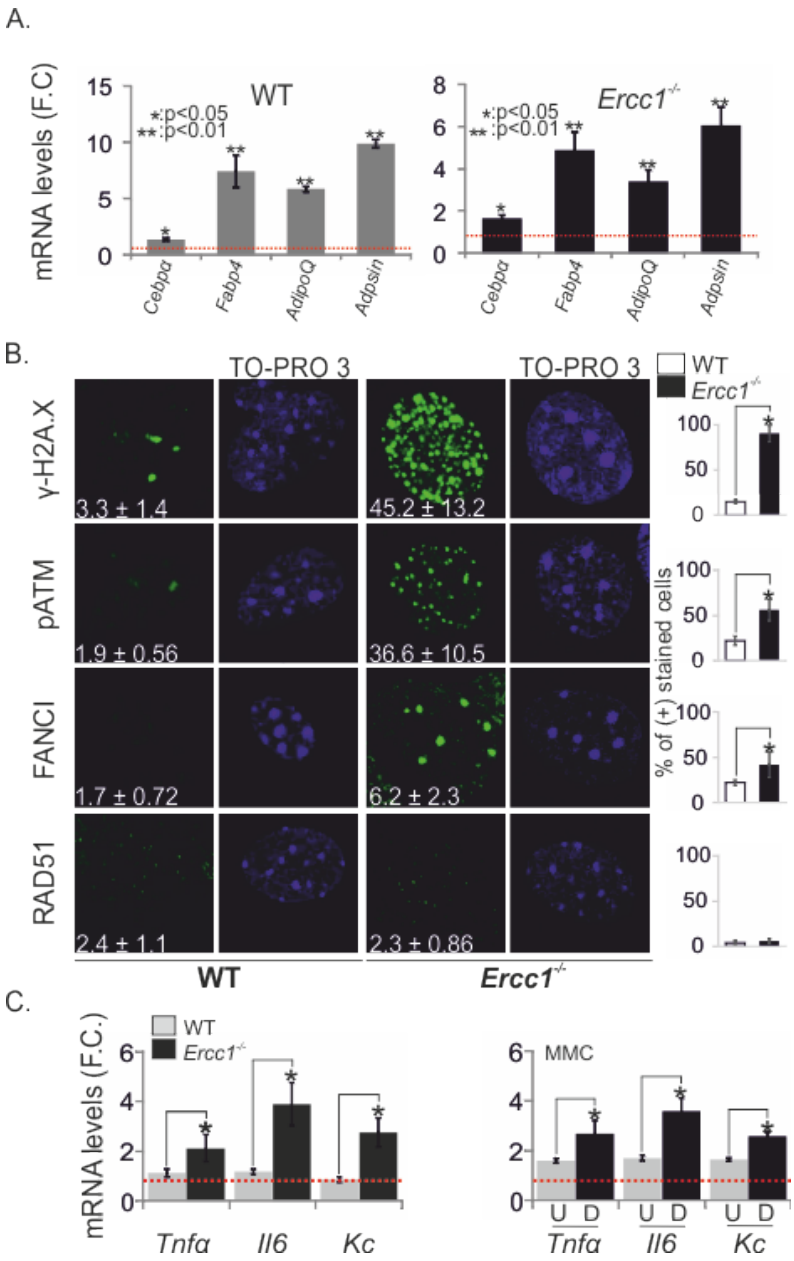

Figure 15 Pro-inflammatory signalling is cell-autonomous in *Ercc1*$^{-/-}$ adipocytes. (A). Quantitative (q) PCR mRNA levels of genes marking the differentiation status of WT and *Ercc1*$^{-/-}$ adipocytes. Red dotted line: undifferentiated controls. (B). Immunofluorescence detection and quantification of γ-H2A.X-, phospho-ATM- and FANCI-containing foci in unchallenged WT and *Ercc1*$^{-/-}$ adipocytes. Numbers in lower left corner indicate average number of foci per nucleus ±S.E.M. (C). qPCR mRNA levels of *Tnfα*, *Il6* and *Kc* genes in WT, *Ercc1*$^{-/-}$ or MMC-treated WT adipocytes (as indicated). Red dotted line: undifferentiated controls (left) or untreated controls (right). Topro: nuclei, error bars indicate S.E.M., * p-value≤0.05.

undifferentiated MEFs. The macrophage pro-inflammatory gene expression observed in 4 months old aP2-*Ercc1*$^{F/-}$ WAT depots rather reflects their activation state and not an Ercc1-dependent DNA damage response.

DNA damage signalling triggers histone changes associated with active pro-inflammatory gene transcription

To gain further mechanistic insight into how the accumulation of persistent DNA damage foci leads to the transcriptional activation of *Tnfα*, *Il6* and *Kc* in *Ercc1*$^{-/-}$ adipocytes, we carried out a series of chromatin immunoprecipitation (ChIP) assays to examine the status of *Il6*, *Tnfα* and *Kc* promoters. Our analysis revealed substantial loss of repressive histone H3K9 and H3K27 trimethylation marks and a concomitant increase in activating acetylated histone H3K9 and H3K4 trimethylation marks in *Ercc1*$^{-/-}$ adipocytes compared to *Ercc1*$^{-/-}$ MEFs and in MMC-treated wt adipocytes compared to untreated controls (**Figure 16A, B**). Wt adipocytes also displayed an increase in activating histone marks compared to undifferentiated MEFs; however, unlike the *Ercc1*$^{-/-}$ adipocytes, repressive histone H3K9 and H3K27 trimethylation marks were maintained or increased in these cells (data not shown), possibly marking their potential to trigger a similar response upon DNA damage signalling. Thus, spontaneous DNA damage due to a DNA repair defect or exposure of adipocytes to the genotoxin MMC triggers histone post-translational modifications associated with active transcription in *Il6*, *Tnfα* and *Kc gene* proximal promoters.

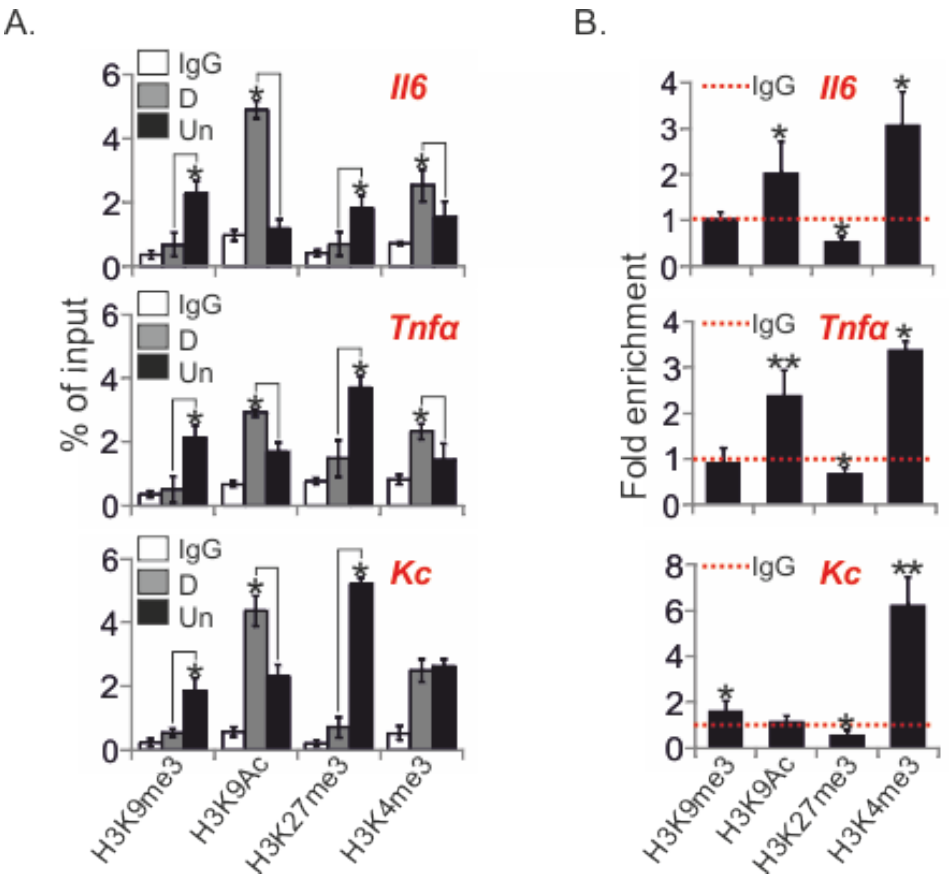

Figure 16 DNA damage in adipocytes triggers activating histone marks in pro-inflammatory gene promoters. (A). ChIP signals (shown as percent of input) of repressive H3K9me3, H3K27me3 and activating H3K9Ac, H3K4me3 histone marks on *Il6*, *Tnfα* and *Kc* proximal promoters in *Ercc1*$^{-/-}$ adipocytes and undifferentiated controls. IgG: control immunoglobulin signal. (B). ChIP signals (shown as fold enrichment) of repressive H3K9me3, H3K27me3 and activating H3K9Ac, H3K4me3 histone marks on *Il6*, *Tnfα* and *Kc* proximal promoters in MMC-treated wt adipocytes. ChIP signals were normalized to input and expressed as fold enrichment over those obtained from untreated controls. Red dotted line: IgG control signal set to 1. Error bars indicate S.E.M., * p-value≤0.05, ** p-value≤0.01.

Persistent DNA damage signalling triggers the transcriptional de-repression of *Il6, Tnfα* and *Kc*

There is mounting evidence that at least some pro-inflammatory cytokines are in a poised, yet repressed transcriptional state. Repression of active transcription is mediated by the recruitment of a co-repressor complex containing the nuclear receptor co-repressor (NCoR1) or the related silencing mediator of retinoic acid and thyroid hormone receptors (SMRT) on promoters (Perissi *et al*. 2010). PPARγ, whose protein and mRNA levels were substantially decreased in aP2-*Ercc1*$^{F/-}$ WAT depots, recruits SMRT and NCoR1 in the absence of ligand and these co-repressors are capable of down-regulating PPARγ-mediated transcriptional activity. In addition, NCoR1 and SMRT mediate active repression of their respective target genes through the recruitment of additional co-repressor molecules, including the histone deacetylase HDAC3 (Perissi *et al*. 2010). Importantly, exposure of wt adipocytes to MMC led to the suppression of *Pparγ2* but not *Pparγ1* mRNA levels (**Figure 17A**). This and the up-regulation of *Il6, Tnfα* and *Kc* pro-inflammatory cytokine mRNA levels in *Ercc1*$^{-/-}$ fat depots prompted us to examine

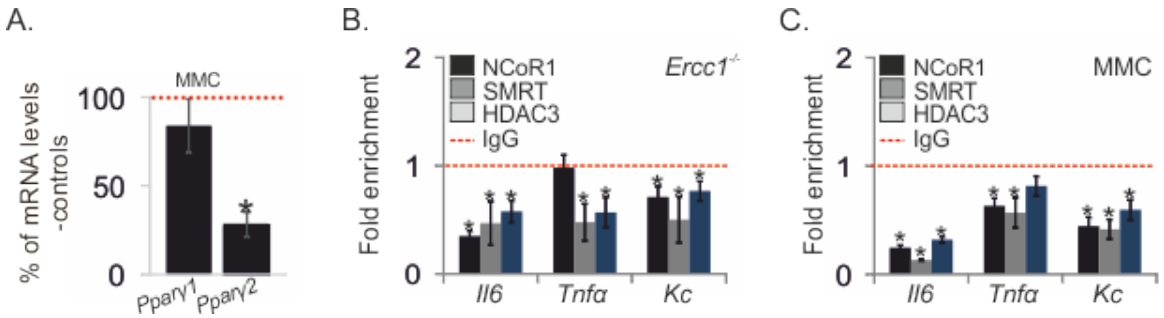

Figure 17 DNA damage triggers pro-inflammatory gene promoter de-repression. (A). Quantitative (q) PCR mRNA levels of *Pparγ1/2* genes in MMC-treated wt adipocytes. Red dotted line: untreated controls. (B). ChIP signals (shown as fold enrichment) of co-repressors NCoR1, SMRT and HDAC3 on *Il6*, *Tnfα* and *Kc* proximal promoters in *Ercc1*$^{-/-}$ adipocytes. ChIP signals were normalized to input and expressed as fold enrichment over those obtained from undifferentiated controls. Red dotted line: IgG control signal set to 1. (C). ChIP signals (shown as fold enrichment) of co-repressors NCoR1, SMRT and HDAC3 on *Il6*, *Tnfα* and *Kc* proximal promoters in MMC-treated wt adipocytes. ChIP signals were normalized to input and expressed as fold enrichment over those obtained from untreated controls. Red dotted line: IgG control signal set to 1. Error bars indicate S.E.M., * p-value≤0.05.

whether the co-repressor complex NCoR1-SMRT-HDAC3 is released from promoters in *Ercc1*$^{-/-}$ adipocytes or upon exposure of wt adipocytes to MMC. With the exception of NCoR1 for *Tnfα* promoter in *Ercc1*$^{-/-}$ adipocytes, we found substantially lower ChIP signals for the NCoR1, SMRT and HDAC3 on *Il6*, *Tnfα* and *Kc* promoters in *Ercc1*$^{-/-}$ adipocytes or MMC-treated wt adipocytes relative to corresponding controls (**Figure 17B, C**). These findings, together with the down-regulation of *Pparγ2* mRNA levels in MMC-treated wt adipocytes, suggest a functional link between DNA damage and the transcriptional down-regulation of nuclear receptors in adipocytes. Thus, defective DNA repair or exposure of wt adipocytes to a cross-linking agent triggers the transcriptional de-repression of pro-inflammatory cytokines.

The accumulation of phosphorylated ATM in the cytoplasm of 4 months old aP2-*Ercc1*$^{F/-}$ adipocytes prompted us to test whether ATM is required for the DNA damage-driven transcriptional de-repression of *Il6, Tnfα* and *Kc* in adipocytes. Inactivation of ATM by exposing MMC-treated adipocytes to KU-55933 inhibitor known to ablate DNA damage-induced phosphorylation of ATM substrates (Ding *et al*. 2006) significantly abrogated the release of repressor complexes from promoters and abolished the transcriptional induction of *Il6, Tnfα* and *Kc* mRNA levels in these cells (**Figure 18A, as indicated**). We also exposed MMC-treated adipocytes to ATR/CDK inhibitor (i.e. NU6027) known to inhibit ATR kinase without interfering with irradiation-induced auto-phosphorylation of DNA-PK or ATM. Inactivation of ATR led to similar results with those seen upon ATM inactivation, albeit to a smaller magnitude (**Figure 18A**). Thus, while ATR may contribute to the transcriptional de-repression of promoters, ATM is essential in linking the nuclear DDR signaling to the transcriptional activation of pro-inflammatory cytokines in aP2-*Ercc1*$^{F/-}$ WAT depots. Similarly, activation of the anti-inflammatory PPARγ by

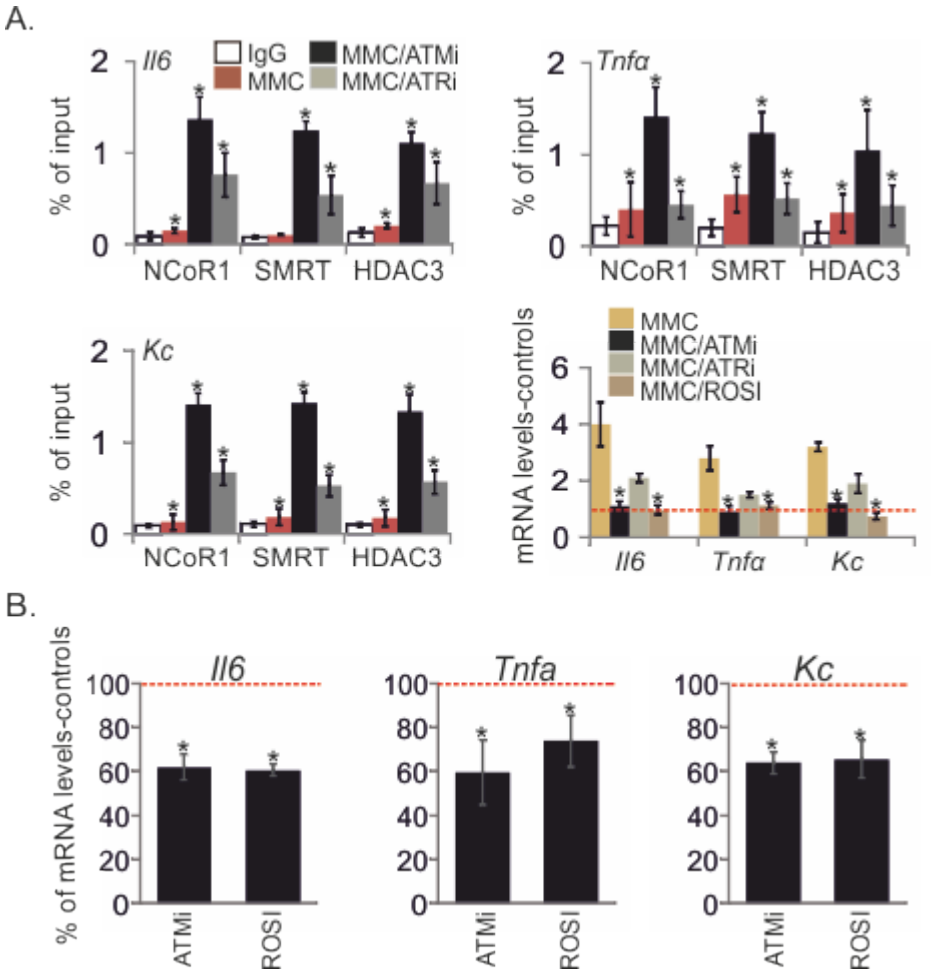

Figure 18 ATM/ATR inhibition abrogates the DNA damage-induced pro-inflammatory signalling. (A). ChIP signals (shown as percent of input) of co-repressors NCoR1, SMRT and HDAC3 on *Il6*, *Tnfα* and *Kc* proximal promoters (as indicated) upon ATM or ATR inhibition in MMC-treated wt adipocytes or not and quantitative (q) PCR mRNA levels of *Il6*, *Tnfα* and *Kc* genes upon ATM/ATR inhibition or PPARγ activation in MMC-treated wt adipocytes or not. IgG: control immunoglobulin signal. Red dotted line: untreated controls. (B). qPCR mRNA levels of *Il6*, *Tnfα* and *Kc* genes upon ATM inhibition or PPARγ activation in *Ercc1*$^{-/-}$ adipocytes. Red dotted line: untreated controls. Error bars indicate S.E.M., * p-value≤0.05.

exposing MMC-treated adipocytes to Rosiglitazone, a PPARγ agonist, significantly abrogated the transcriptional induction of *Il6*, *Tnfα* and *Kc* mRNA levels (**Figure 18A, as indicated**). To test whether ATM and PPARγ play similar roles in *Ercc1*$^{-/-}$ adipocytes, we inhibited ATM or activated PPARγ in *Ercc1*$^{-/-}$ adipocytes; importantly, treatment of *Ercc1*$^{-/-}$ adipocytes with KU-55933 inhibitor or Rosiglitazone significantly abrogated the transcriptional induction of *Il6*, *Tnfα* and *Kc* mRNA levels compared to untreated controls

(**Figure 18B**), a finding that was also confirmed in ATMi-treated adipocyte culture media for TNF-α protein levels (data not shown). Finally, we observe a similar response in naturally aged tissues, where *Ercc1* mRNA levels are significantly decreased whereas *Il6, Tnfa* and *Kc* mRNA levels are significantly increased when 110 week old wt fat depots are compared to 6-week old ones (**Figure 19A**). Thus, our findings provide a model in which persistent DNA damage in aP2-*Ercc1*$^{F/-}$ fat depots *in vivo* and in adipocytes *ex vivo* triggers the induction of pro-inflammatory cytokines by promoting transcriptionally active histone marks and the dissociation of nuclear receptor co-repressor complexes from promoters.

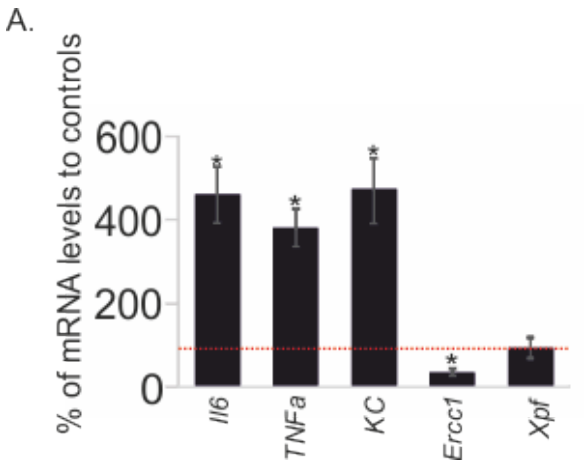

Figure 19 Pro-inflammatory signalling in naturally aged white adipose tissue. (A). Quantitative (q) PCR mRNA levels of *Il6, Tnfα, Kc, Ercc1* and *Xpf* genes in the white adipose tissue of 110 weeks old mice. Red dotted line: young 6 weeks old tissues. Error bars indicate S.E.M., * p-value≤0.05.

Discussion

ERCC1 deficiency results in the manifestation of a great variety of symptoms in patients and accompanying mouse models (Weeda *et al*. 1997; Niedernhofer *et al*. 2006; Jaspers *et al*. 2007). Until recently, it has proved difficult to decipher how DNA damage accumulation, in view of the NER defect, leads to the manifestation of tissue-specific pathology. In view of the random nature of DNA damage that indiscriminately affects all cell types, it also remains unclear how mutations in *Ercc1* results in distinct phenotypic outcomes with prominent pathological features in some, but not all tissues (Andressoo *et al*. 2006). Apart from the growth defect, which has been attributed to an ERCC1/XPF-dependent transcriptional defect in genes that regulate the somatotroph, lactotroph and thyrotroph axes in the liver (Kamileri *et al*. 2012b), other symptoms that resemble premature ageing phenotypes lack a mechanistic explanation. In the present study, we uncover a causative link between irreparable DNA lesions in adipocytes, persistent DNA damage signalling and the dramatic loss of adipose tissue that is observed upon *Ercc1* deletion. Using the *Ercc1*$^{-/-}$ mice, we show that already at P15, the white adipose tissue (WAT) mass is significantly reduced in all the depots examined. However, these mice fail to develop normally, present several progeroid symptoms and die before weaning, possibly of liver failure (Neidernhofer *et al*. 2006). To exclude the possibility of an indirect, systemic effect that leads to adipose tissue loss, we generated a tissue-specific *Ercc1*$^{-/-}$ mouse model, by restricting *Ercc1* deletion only in adipose tissue (aP2-*Ercc1*$^{F/-}$ mice). Importantly, the aP2 gene promoter is active in the mature adipocyte (Tang *et al*. 2008), allowing us to study the role of irreparable DNA lesions in a functional adipose tissue, without interfering with its differentiation. In line, the adipose tissue-specific ko

mice develop normally, are fertile and show no gross phenotypic abnormalities up to two months of age, in contrast with the growth-defective, short-lived *Ercc1*$^{-/-}$ mice. Beginning at 3 months of age, however, the mice appear thinner; their adipose tissue depots are also visibly reduced compared to littermate controls. Scanning electron microscopic observation of their WAT depots at 4 months of age revealed a gross degenerative phenotype, including basement membrane rupture, adipocyte depletion, extensive fibrosis and ciliae reappearance (**Figure 5**). The degenerative features observed in the tissue-specific ko mice, which resemble lipodystrophy, support the hypothesis that *Ercc1* deletion in adipocytes alone is sufficient to cause fat depletion.

The aP2-*Ercc1*$^{F/-}$ mouse as a model of lipodystrophy

The aP2-*Ercc1*$^{F/-}$ mice develop metabolic abnormalities that have been described in other lipodystrophic animal models and include severe defects in glucose and lipid homeostasis (Fiorenza *et al*. 2011). The 4 months old aP2-*Ercc1*$^{F/-}$ mice show hypertriglyceridaemia, ectopic lipid accumulation in skeletal muscle and heart, higher insulin production in the pancreas and hyperinsulinaemia, lower levels of the adipokine adiponectin and glucose intolerance, features that are observed in type II diabetes mellitus and the metabolic syndrome often related to obesity (Baker *et al*. 2011). In order to identify the transcriptional responses that are elicited upon *Ercc1* deletion in white adipose tissue (WAT), we scanned the WAT transcriptional profiles of 15-day old *Ercc1*$^{-/-}$ mice. This led to the detection of five over-represented biological processes, namely a response to DNA double-strand breaks, pro-inflammatory and nuclear receptor signalling, growth factor signalling and an oxidative stress response. Comparison of the *Ercc1*$^{-/-}$ WAT gene expression profiles to those derived from the *Pparγ*$^{Ldi/+}$ mouse, a known lipodystrophic

model, revealed that a lipodystrophic signature is established early in *Ercc1*$^{-/-}$ mice. The *Pparg*$^{ldi/+}$ mouse was generated by substituting the Pparγ gene with a tetracycline-inducible *Flag-Pparγ1* cDNA transgene (Kim *et al*. 2007). This transgene conferred dominant lipodystrophy in mice, which could be reversed upon doxycycline treatment. The *Pparγ*$^{Ldi/+}$ mouse exhibited a marked loss of WAT depots, fibrosis and leukocyte infiltration in adipose tissue, accompanied by dyslipidaemia, insulin resistance and pancreatic islet hypertrophy, abnormal metabolic features which are often associated with lipodystrophy (Kim *et* al. 2007). Thus, two disparate animal models such as the *Ercc1*$^{-/-}$ and *Pparγ*$^{Ldi/+}$ mice, share 450 commonly misexpressed genes. Within this shared gene set, our analysis revealed a number of pathways previously reported to be affected during lipodystrophy that were commonly over-represented, including the TNF/NFκB, PI3K/AKT pathways, HMGB1 signalling, transcriptional repression and activation by the Retinoic Acid receptor (RAR). Confirmation of these findings in the tissue-specific ko mice (**Figures 10-13**), in parallel with the degenerative loss of adipose tissue and the accompanying metabolic abnormalities that they present, suggests that the aP2-*Ercc1*$^{F/-}$ mice represent a valid model to study lipodystrophy. Cachexia has been identified as a prominent feature of NER-deficient patients and corresponding mouse models (de Boer *et al*. 2002; Niedernhofer *et al*. 2006; Kamenisch *et al*. 2010). However, evidence linking this phenotype to metabolic syndrome (MetS) and the development of diabetes is currently lacking. MetS refers to a cluster of conditions often associated with obesity and includes elevated plasma triglyceride levels, increased blood pressure or increased fasting plasma glucose levels (Kennedy *et al*. 2010). MetS may result from over-nutrition, insulin resistance and/or chronic low-grade inflammation of adipose tissue (Baker *et al*. 2011) and it is associated with increased risk of developing diabetes or suffering from heart attack or stroke (Kennedy *et al*. 2010). However, lipodystrophy has also been associated

with MetS (Fiorenza *et al*.2011). Lipodystrophic mouse models provide evidence towards this direction: they develop hyperlipidaemia, hepatic steatosis, insulin resistance or hypertension (Kennedy *et al*. 2010). The aP2-*Ercc1*$^{F/-}$ mice develop a similar pathology and represent the first NER-deficient mouse model linking genomic instability in adipose tissue to the manifestation of metabolic complications. In previous studies, the *Werner helicase* (*WRN*), which is implicated in telomere maintenance and irradiation-induced DNA repair, and the *laminA* (*LMNA*)/metalloproteinase *ZMPSTE24* genes, which are involved in DSB repair, have been shown to cause the progeroid syndromes Werner and Mandibuloacral dysplasia (MAD), respectively and have also been linked to the manifestation of metabolic abnormalities in patients or mouse models (Schumacher *et al*. 2008; Ciccia and Elledge, 2010). These factors affect both genomic stability and metabolic homeostasis and thus provide an additional link between DNA damage and MetS. However, the molecular mechanisms linking genomic instability to the development of metabolic complications remain unclear. In the aP2-*Ercc1*$^{F/-}$ mice, metabolic abnormalities arise later in life, well after persistent DDR is evident in their adipose tissue. Thus, it is likely that they represent a secondary, systemic effect of adipose tissue dysfunction due to DNA damage accumulation in mature adipocytes. The recently identified role of ERCC1/XPF in facilitating transcription (Le May *et al*. 2010; Kamileri *et al*. 2012b) could provide additional insight. For instance, involvement of these factors in regulating transcription of adipokines, such as adiponectin, or other factors that are instrumental in maintaining adipose tissue-mediated metabolic homeostasis could also explain the development of metabolic abnormalities upon *Ercc1* ablation. Although our study provides a causative link between persistent DNA damage and adipose tissue inflammation that leads to metabolic complications, it cannot exclude the possibility of an additional, ERCC1-mediated transcriptional problem that contributes to the phenotype. It

would be interesting to see whether *Ercc1* deletion in other cell types that are instrumental in regulating the body's energy balance would result into similar phenotypic abnormalities.

Persistent DDR triggers a cell-autonomous auto-inflammatory response in the adipose tissue

Not surprisingly, the aP2-*Ercc1*$^{F/-}$ mice induce a DNA damage response in their adipose tissue, as exemplified by the accumulation of nuclear DNA damage/repair foci formed by phosphorylated H2A.x (γ-H2A.x), FANCI and RAD51. Activated ATM (phospho-ATM) was also detectable in these tissues with a predominantly cytoplasmic localisation. Shuttling of phosphorylated ATM to the cytoplasm upon genotoxic stress has been previously linked to NEMO-mediated IκB degradation and NF-κB gene target transcriptional activation (Wu *et al*. 2006). The presence of DNA repair foci together with the transcriptional up-regulation of several DNA repair genes mark the existence of persistent DNA damage signalling in the adipose tissue of the aP2-*Ercc1*$^{F/-}$ mice. Persistent DDR coincides with the release of HMGB1, a chromatin-associated factor that serves as an activator of Toll-like receptors (Park *et al*. 2004), and is closely followed by pro-inflammatory molecule expression and the infiltration of adipose tissue by innate immune cells (**Figures 10-13**). Permanently arrested i.e. senescent cells are known to trigger a response called senescence-associated secretory phenotype (SASP); senescent cells secrete pro-inflammatory molecules that likely signal their compromised state to surrounding cells and alter their microenvironment (Coppe *et al*. 2008). However, it has been shown that persistent DNA damage signalling by means of activated ATM, CHK2 and the presence of several DNA repair factors in chromatin structures that persist in the

nucleus is indispensable for the secretion of pro-inflammatory molecules (Rodier *et al*. 2009, Rodier *et al*. 2011). Additionally, the expression of a cyclin-dependent kinase inhibitor $p16^{INK4a}$, which is known to cause cellular senescence, did not cause induction of pro-inflammatory molecule secretion, although detection of other senescence markers was evident (Rodier *et al*. 2009). Persistent DDR and pro-inflammatory cytokine production irrespective of senescence in the adipose tissue of the aP2-$Ercc1^{F/-}$ mice further supports these studies, as we were unable to detect any senescent adipocytes in these mice. Collectively, these data suggest that, unlike senescence, it is the DNA damage response signalling that triggers the release of pro-inflammatory molecules. In the context of a particular tissue, DNA damage, unequivocally induces a protective response that is directed inwards by arresting the cell cycle and engaging the respective DNA repair machinery to faithfully restore the compromised genome (Dasika *et al*. 1999; D' Amours and Jackson, 2002). Interestingly, the same DNA damage response seems to also trigger a response that is directed outwards and is aimed at alerting the surrounding environment of cellular damage. This notion is also supported by the recent finding that in the *C. elegans* germline, genotoxic stress induces the expression of putative pro-inflammatory peptides which activate an innate immune response in the worm soma (Ermolaeva *et al*. 2013). In keratinocytes, UV-mediated activation of the inflammasome, a cytoplasmic multi-protein innate immune complex, leads to the release of pro-inflammatory IL1β (Feldmeyer *et al*. 2007). Additionally to secreted pro-inflammatory molecules, genotoxic stress has been shown to induce the expression of ligands recognized by the NKG2D (Gasser *et al*. 2005) or the DNAM-1 receptor (Soriani *et al*. 2009) of the Natural Killer (NK) cells, in an ATM/ATR-dependent manner. Together with HMGB1, which activates tissue-resident macrophages expressing Toll-like receptors (Medzhitov, 2010), these immunomodulatory

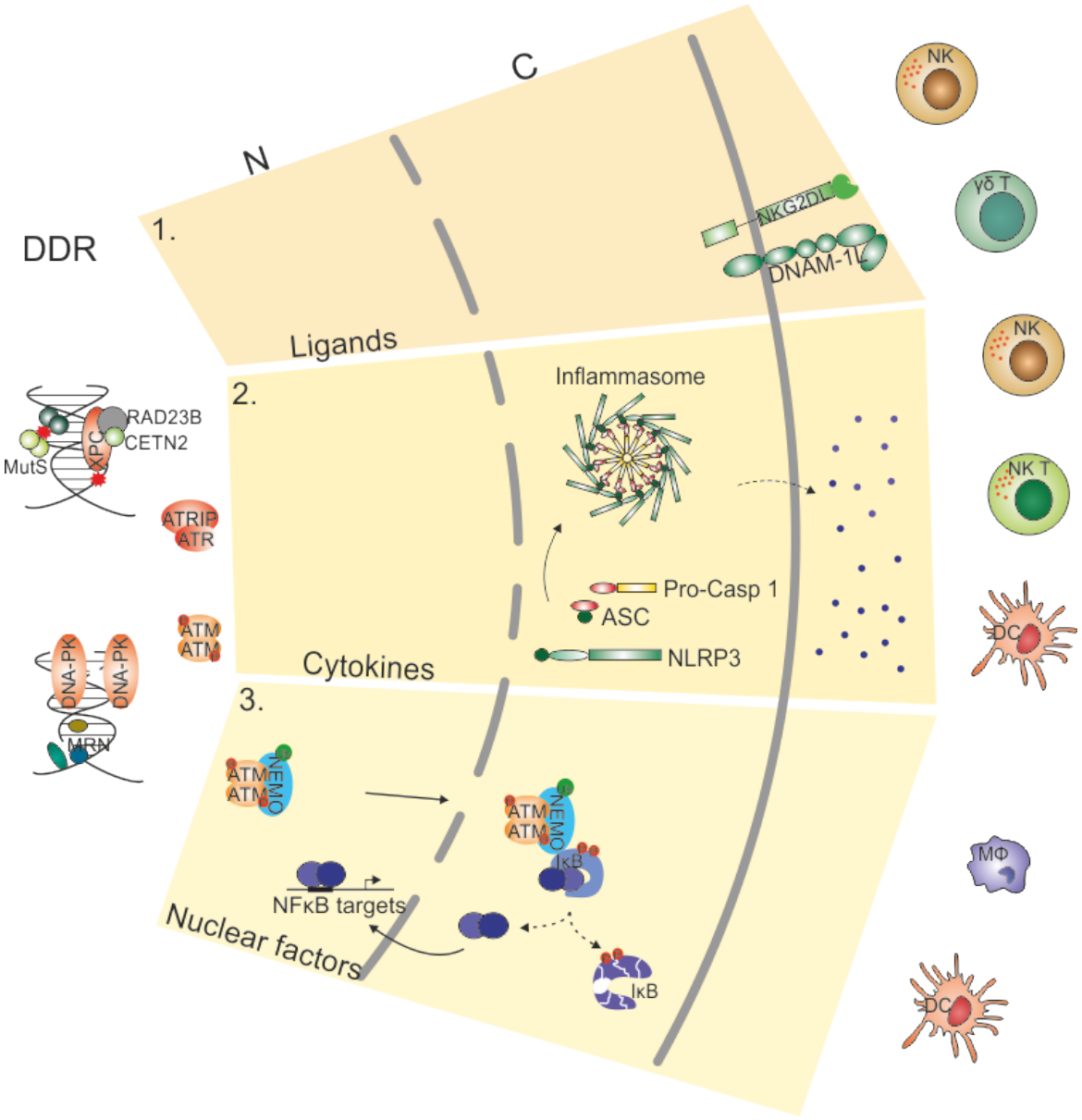

Figure 20 DNA damage and immunity. DNA damage detection by specific complexes (MutS, XPC/RAD23B/CETN2, DNA-PK, MRE11/RAD50/NBS1 – MRN) or signaling by ATM (Ataxia Telangiectasia Mutated) and ATR (ATM and Rad3-related) following lesion recognition in the nucleus, can activate innate immune cell responses in several ways. Cells exposed to DNA damaging agents express cell surface ligands for the NKG2D and DNAM-1 receptors (1), which are found on NK (Natural Killer) and γδ T cells. DDR (DNA damage response) can also trigger the formation of a cytoplasmic structure, the inflammasome, and the release of cytokines in the extracellular space (2), which are perceived as activating signals by several innate immune cells. In (3), within the nucleus, activated ATM associates with NEMO (NF-κB Essential Modulator) and triggers its ubiquitylation and nuclear export. In the cytoplasm, NEMO phosphorylates IκB (Inhibitor of κB), which is subsequently degraded and released NF-κB (Nuclear Factor kappa-light-chain-enhancer of activated B cells) moves to the nucleus to activate expression of target genes. NF-κB targets can activate innate immunity through macrophages (Mφ) and dendritic cells (DC). N: nucleus, C: cytoplasm.

factors serve as potent inducers of an innate immune response that aims at counteracting noxious stimuli (**Figure 20)**.

Adipose tissue is a potent inflammatory organ harbouring a large number of tissue resident macrophages and other innate and adaptive immune cells. It is thus considered a tertiary lymphoid organ (Chawla *et al*. 2011), able to initiate a pro-inflammatory response which can become systemic, often with adverse metabolic effects. In insects, metabolism and immunity are tightly correlated and they are regulated by the fat body, an organ analogous to the mammalian liver and adipose tissue (DiAngelo *et al*. 2009; Clark *et al*. 2013). In mammals, these organs remain distinct and have evolved specialized functions. However, both liver and adipose tissues contain resident macrophages, facilitating a continuous and dynamic interaction between metabolism and immune homeostasis (Hotamisligil, 2006). Conceivably, a stressor, such as the DNA damage response, will activate an inflammatory response faster and in a more efficient way in adipose tissue, merely due to cellular proximity. Under physiological conditions, innate immune responses attempt to restore homeostasis by triggering cell clearance and regeneration (Medzhitov, 2010). However, in view of the DNA repair defect in the aP2-*Ercc1*$^{F/-}$ mice and the persistent DDR that is initiated in the adipose tissue, this beneficial role triggers a chronic inflammatory response that ultimately leads to tissue degeneration. Chronic immune cell infiltration destroys the tissue microenvironment and can also lead to exhaustion of progenitor cell pools, as pro-inflammatory molecules can trigger their differentiation as well as the degeneration of their niche by extensive extracellular matrix deposition (Freund *et al*. 2010).

At the molecular level, pro-inflammatory genes must be actively repressed in cell types that should not express them, but at the same time retain the ability of a rapid induction, upon proper stimulation. Such a function can be carried out by transcriptional co-repressors. Factors such as NCoR/SMRT (Nuclear receptor Co-Repressor 1/Silencing Mediator of Retinoic acid and Thyroid hormone receptor) and related histone deacetylases associate with the anti-inflammatory PPARγ (Peroxisome Proliferator-Activated Receptor γ) to suppress pro-inflammatory gene transcription (Straus and Glass, 2007). In an *Ercc1*-deficient background or in wt adipocytes exposed to an exogenous DNA damaging agent, pro-inflammatory gene promoters are de-repressed; NCoR1/SMRT/HDAC3 are released from the promoters in an ATM-dependent manner, together with a concomitant increase in activating and a decrease in suppressive histone post-translational modifications (**Figures 16-18**). The finding that activating histone PTMs are enriched in pro-inflammatory gene promoters of wt adipocytes, although suppressive histone PTMs and the co-repressor complex are still present, supports the idea of a poised chromatin state in these cells, awaiting a relevant stimulus to trigger the release of repressors and allow the transcription of pro-inflammatory molecules. In *Drosophila*, genome-wide analysis of RNA Pol II promoter occupancy revealed several clusters of genes which dynamically respond to environmental or developmental stimuli to be in a poised state, awaiting relevant stimuli to engage productive transcription (Muse *et al*. 2007). Thus, the default state of pro-inflammatory genes could be towards expression in an inflammatory organ like adipose tissue, but in the absence of an intrinsic or extrinsic insult, they would rather be kept repressed, so as to avoid untimely activation of an innate immune response.

Concluding Remarks

In the present study, we show that *Ercc1* deletion induces a persistent DDR leading to pro-inflammatory gene promoter de-repression in adipocytes and an auto-inflammatory response that ultimately leads to adipose tissue degeneration as well as the development of secondary adverse metabolic effects in the aP2-*Ercc1*$^{F/-}$ mice. These findings provide direct *in vivo* link between DNA damage accumulation and adipose tissue-specific pathology that is observed in prematurely as well as naturally aged individuals (**Figure 21**). A number of additional studies have uncovered a causal link between genotoxic stress and the activation of innate immune responses (Gasser *et al*. 2005; Wu *et al*. 2006; Tilstra *et al*. 2012; Ermolaeva *et al*. 2013). Triggering such responses requires signalling through ATM/ATR and MAP kinases (Ermolaeva and Schumacher, 2014). However, if local innate immune activation is the underlying cause of other progeroid features and how these processes resemble normal ageing is still unknown. In order to be able to intervene with particular nodes to prevent or delay age-related disease onset, we need to uncover the mechanistic details that regulate such responses in a tissue-specific manner. The use of high-throughput techniques coupled with sophisticated mouse models could help towards this direction. Recently, we have made use of an efficient *in vivo* tagging method (de Boer *et al*. 2003) and have developed a knock-in mouse model by targeting a short sequence tag at the C-terminus of XPF, the heterodimeric partner of ERCC1 (Karakasilioti, Kosteas and Garinis, unpublished results). The short tag is specifically recognized and biotinylated by a bacterial biotin ligase (de Boer *et al*. 2003; Kamileri *et al*. 2012b). This powerful genetic tool allows us to isolate and characterize the protein complexes that are formed by ERCC1/XPF *in vivo* in several tissues and cell types, under different stress conditions and treatments that activate persistent DNA damage responses or upon natural ageing. Comparison of proteomic profiles from treated and untreated

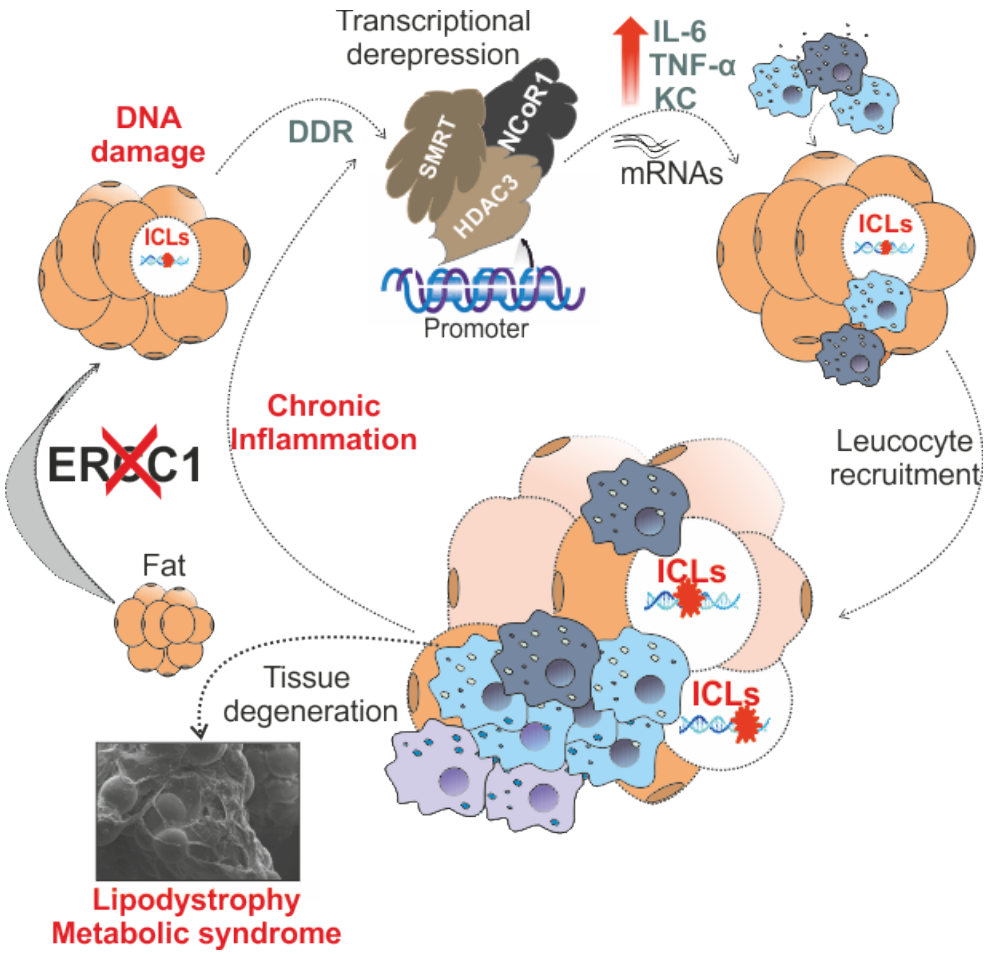

Figure 21 DNA damage triggers a chronic auto-inflammatory response leading to fat depletion in NER progeria. Tissue-specific Ercc1 ablation from adipose tissue induces a persistent DNA damage response and transcriptional de-repression of pro-inflammatory gene promoters. Overexpression of these genes leads to an auto-inflammatory response, infiltration of adipose tissue by innate immune cells and a chronic propagation of this signalling, which ultimately leads to adipose tissue degeneration, lipodystrophy and metabolic syndrome observed in these mice.

(naive) relevant cell types, such as adipocytes or macrophages, could reveal cell-type specific complexes that are formed or dissociate upon exposure to DNA damaging agents or due to intrinsic DNA damage accumulation that occurs during ageing. Discrete nuclear complexes could be coupled with information from additional high-throughput approaches, such as ChIP-sequencing data to identify the genome-wide occupancy of these factors. Whether ERCC1/XPF also has a direct role in transcriptionally regulating

tissue-specific factors that are associated with disease progression could be answered by this approach. Several outcomes of the DDR could be controlled at the post-transcriptional level. Also, the activation of innate immune or other systemic responses happens through inter-cellular communication mediated by secreted factors. Thus, complementary approaches towards the characterization of cell-type specific secreted factors could also contribute to understanding the networks that are perturbed during disease progression. The combination of click chemistry with pulsed stable isotope labelling in cell culture (SILAC) could be used towards this direction (Eichelbaum *et al*. 2012). Understanding the molecular pathways that link NER factors to inflammation or other tissue-specific responses in the mouse will provide insight into tissue-specific pathology and systemic responses that are observed both in progeroid patients and naturally aged individuals. This knowledge could help towards developing new interventions for a healthier lifespan.

Materials and Methods

Mice

The generation of *Ercc1*$^{-/-}$ mice was previously described (Niedernhofer *et al*. 2006). *Ercc1*^{F} mice containing a floxed allele (exons 7-10) of the *Ercc1* gene (Verhagen-Oldenampsen *et al*. 2012) were backcrossed to C57Bl/10 background. *Ercc1*^{F} homozygote mice were crossed with *Fabp4 (aP2)-Cre; Ercc1*$^{+/-}$ mice to obtain inactivation of the *Ercc1* gene in adipocytes. Rosa26-*YFP*$^{st/st}$ mice were crossed with *Fabp4 (aP2)-Cre transgenic mice to obtain YFP expression in adipocytes.* Pups were genotyped for the respective alleles using standard procedures and primer pairs outlined in Table 1.

Table 1. Genotyping primers sequences.

Primer	Sequence	Allele
F25732	TCAAAGTATGGTAGCCAAGGCAGC	Ercc1
432E	TGCAGAGCCTGGGGAAGAACTTCGC	Ercc1
Cre F	GCGGTCTGGCAGTAAAACTATC	Cre
Cre R	GTGAAACAGCATTGCTGTCACTT	Cre
Rosa LC	GCTCTGAGTTGTTATCAGTAAGG	YFP
Rosa R2	GCGAAGAGTTTGTCCTCAACC	YFP
Rosa R3	GGAGCGGGAGAAATGGATATG	YFP

Animal studies

For food and water intake studies, 1.5-month old aP2-*Ercc1*$^{F/-}$ and wt littermate controls (n=5 per genotype) were allowed to standard chow (Certified standard diet 4RF21, Mucedola) and water *ad libitum*. Animals were monitored daily for 4 weeks and their

food and water consumption was measured once per day, morning hours. For insulin tolerance tests (ITT), glucose tolerance tests (GTT), total serum cholesterol, triglyceride and insulin measurements, mice were fasted for six hours prior to injections or serum isolation. For ITT, mice were injected intraperitoneally with 0.75 Units/kg of body weight insulin (Humulin, Ely Lili). For GTT, mice were injected intraperitoneally with 1 g/kg of body weight 35% dextrose solution. Blood glucose levels were determined using a glucometer (Bayer Pharmaceuticals). Serum total cholesterol (Infinity cholesterol, Thermo Scientific) and triglyceride (LabAssay triglyceride, Wako Chemicals) content were determined with colorimetric assays. Serum insulin levels were measured by elisa (Millipore). For BrdU incorporation studies, mice were injected intraperitoneally with 30 mg/kg of body weight BrdU (Sigma) in 1x PBS and sacrificed 48 hours later. For macrophage isolation, macrophages were elicited for four days using 4% thioglychollate broth (DIFCO Laboratories), isolated by peritoneal lavage with 10 ml dMEM per mouse and seeded on coverslips for immunofluorescence or left to adhere and used for RNA isolation. Animals were maintained in grouped cages in a temperature-controlled virus-free facility on a 12-h light/dark cycle, fed by standard chow diet and water *ad libitum*. An independent Animal Ethical Committee at the IMBB-FORTH approved the animal studies.

Scanning electron microscopy

For scanning electron microscopy (SEM), fresh adipose tissue was cut into small blocks. Briefly, tissue was fixed for 2 hours with 2% paraformaldehyde – 2% glutaraldehyde in 0.1 M sodium cacodylate buffer. Samples were post-fixed overnight in 1% osmium tetroxide (OTO method) and dehydrated in a graded series of ethanol. Specimens were

coated in gold, mounted on aluminum stubs and examined with a JEOL JSM6390 LV scanning electron microscope (Peabody, MA) using an accelerating voltage of 15 kV.

Histology

Tissues were embedded in OCT compound or fixed in 4% paraformaldehyde and paraffin-embedded by standard procedures. For lipids staining, OCT-embedded tissues were cryosectioned using a Leica CM 1850 cryostat, fixed in 10% formalin, stained with Oil Red O (Sigma) and counterstained with Harris's Haematoxylin (Sigma). For insulin production, paraffin-embedded pancreata were sectioned using a Leica RM 2125 microtome, de-paraffinized and re-hydrated, boiled in 10 mM Sodium Citrate buffer for antigen retrieval, stained with anti-insulin antibody (Cell Signaling Technology) and visualized with DAB chromogen (Sigma).

Microarrays and quantitative real-time PCR analysis

Standard procedures were used to obtain total RNA (Qiagen) from the adipose tissue of wt and *Ercc1*$^{-/-}$ animals (n=4). For genome-wide expression analysis, double stranded cDNA and biotin labelled cRNA were produced according to the instructions of the manufacturer (Affymetrix, USA). Fragmented cRNA preparations were hybridized to full mouse genome oligonucleotide arrays (430 V2.0; Affymetrix, USA). Initial data extraction and normalization within each array was performed by means of the GCOS software (Affymetrix). Microarrays complied with the Minimum Information for Microarray Experiments (MIAME) and are available at ArrayExpress (E E-MEXP-3930). All qPCR reactions were performed at least in triplicates using SYBR GreenI (Sigma) and

Platinum Taq polymerase (Invitrogen). Generation of specific PCR products was confirmed by melting curve analysis. Primer pairs were tested with a logarithmic dilution cDNA to generate a linear standard curve (crossing point (CP) plotted versus log of template concentration), which was used to calculate the primer pair efficiency (E 10(−1/slope)). For data analysis, the second derivative maximum method was applied, and induction of target cDNA was calculated according to the following formula: (Etarget ΔCP(cDNAuntreated cDNAtreated)target)/ (EcontrolΔCP(cDNAuntreated-cDNAtreated)control).

Gene Ontology Classification and Overrepresentation of Biological Themes

All significant gene entries were subjected to GO classification (http://www.geneontology.org). Significant overrepresentation of GO-classified biological processes was determined by comparing the number of genes in a given biological process that were significantly differentially expressed in a particular mouse strain to the total number of the genes relevant to that biological process printed on the array (Fisher exact test, $p \leq 0.01$ False discovery rate (FDR) ≤ 0.1) using the publicly accessible software Ease and/or DAVID (http://david.abcc.ncifcrf.gov/summary.jsp). Due to the redundant nature of GO annotations, we employed kappa statistics to measure the degree of the common genes between two annotations and heuristic clustering to classify the groups of similar annotations according to kappa values (http://david.abcc.ncifcrf.gov/summary.jsp). Significant overrepresentation of pathways and gene networks was determined by DAVID (http://david.abcc.ncifcrf.gov/summary.jsp; through BBID, BIOCARTA and KEGG

annotations) as well as by means of the ingenuity pathway analysis software (www.ingenuity.com).

Data analysis

Data mining, statistical and bioinformatics analysis was performed by means of the statistical software IBM SPSS Statistics 19 (IBM, NY, USA), Spotfire (Tibco, CA, USA), Partek (Partek Incorporated, MO, USA) and R-statistical package (www.r-project.org/).

Immunostainings

Immunofluorescence experiments were performed as previously described (Garinis *et al*. 2005; Nishimura *et al*. 2007) and visualized with a Leica TCS SP2 SE confocal microscope. Briefly, cells were seeded on coverslips and cultured as needed, fixed in 4% formalin and post-fixed in methanol. Non-specific binding was blocked with 1% BSA. Cells were incubated with primary antibodies overnight and secondary antibodies and nuclear couterstain (TO-PRO-3, Molecular Probes) for 1 hour 30 minutes. Adipose tissues were cut in small blocks, fixed in 10% formalin with 1% BSA for 30 minutes, permeabilized with 0.1% saponin and blocked with 3% bovine serum and 1% BSA for 1 hour. Tissue fragments were incubated with primary antibodies overnight in the presence of 0.1% saponin/1% BSA and with secondary antibodies and nuclear and/or lipid droplet counterstains (BODIPY, Molecular Probes) for 1 hour 30 minutes, in the presence of 0.1% saponin/1% BSA. For necrotic cell death detection, tissue fragments were stained with isolectin, bodipy and to-pro-3 (Molecular Probes) for 1 hour without prior fixation, in the presence of 1% BSA to avoid adipocyte rupture. For brdU incorporation detection,

fixed tissue fragments were incubated in 0.1N HCl for 1 hour at 37 ˚C, prior to blocking and permeabilization.

ChIP assays and antibodies

For ChIP assays, cells were crosslinked with 1% formaldehyde. Isolated chromatin was sonicated on ice using an Ultrasonic homogenizer Labsonic (Startorius Stedim biotech). Samples were immunoprecipitated with antibodies and protein G Sepharose beads (Millipore) at 4^{o}C overnight and washed sequentially. Crosslinking was heat reversed and purified DNA fragments were analyzed by qPCR using sets of primers targeting different regions of *Il6, Tnfα and Kc* genes. Antibodies against TFIIB (C-18), NCoR (C-20), SMRT (H-300), HDAC3 (H-99), ERCC1 (D-10), XPF (M-16), FANCI (H-102) and beta-ACTIN (H-196) were from SantaCruz Biotechnology, p-H2AX Ser139, RAD51, p-ATM, H3K9me3 and H3K27me3 were from Millipore, H3K4me3 and H3K9Ac were from Abcam, anti-BrdU, MAC3 and iNOS-FITC from BD Pharmingen, HMGB1 from BioLegend and MAC1, CD45, ICAM-1, VCAM and PECAM-1 were from DSHB. IB4 isolectin, BODIPY®, TO-PRO®-3 iodide and secondary anti-mouse, anti-rabbit, anti-rat and anti-goat AlexaFluor-conjugated antibodies were from Molecular Probes. Secondary anti-mouse and anti-rabbit HRP-conjugated antibodies were from Millipore and secondary anti-goat HRP-conjugated antibody was from SantaCruz Biotechnology. The CD11b, CD45, ICAM-1, VCAM and PECAM-1 antibodies were obtained from the Developmental Studies Hybridoma Bank developed under the auspices of the NICHD and maintained by The University of Iowa, Department of Biology, Iowa City, IA 52242.

Protein Extraction

For detection of nuclear protein levels, adipose tissues from 3 mice were pooled together, homogenized in Sucrose A buffer (15 mM Hepes-KOH pH=7.9, 0.32 M Sucrose, 60 mM KCl, 2 mM EDTA, 0.5 mM EGTA, 0.5% BSA, 0.1% NP-40, 0.5 mM DTT, 0.5 mM PMSF, 0.15 mM spermine, 0.5 mM spermidine) to extract nuclei and incubated in RIPA-like buffer (50 mM Tris-Cl pH=8.0, 0.5% NP-40, 0.25% Na-deoxycholate, 400 mM KCl, 1 mM EDTA, 10% glycerol, 1 mM PMSF) for 1 hour to extract nuclear proteins. Nuclear extracts were analysed with SDS-polyacrylamide gels, blotted on nitrocellulose membranes and incubated with corresponding primary and HRP-conjugated secondary antibodies. For Elisa protein detection, whole tissue extracts were prepared by homogenizing adipose tissues from two mice in RIPA buffer (50 mM Tris-Cl pH=8.0, 1% SDS, 0.5% NP-40, 0.25% Na-deoxycholate, 150 mM KCl, 1 mM EDTA, 10% glycerol, 1 mM PMSF) and removing the lipid fraction by centrifugation at 13000 rpm for 15 minutes.

Inflammatory cell counts and FACS analysis

Epididymal adipose tissue was harvested and chopped into fine pieces. Tissue fragments were incubated in 1x HBS buffer supplemented with 2 mg/ml Collagenase (Sigma) for 1 hour at 37 ˚C. The Stromal Vascular fraction was collected by centrifugation and cells were filtered via a 70 nm cell strainer (BD Biosciences) to obtain single cell suspensions. Red blood cells were removed from the cell suspension using ammonium chloride lysis buffer (Sigma). Total white blood cell (WBC) counts per mouse were estimated in the microscope using Kimura stain (Kimura *et al*. 1973). To estimate adipose tissue inflammatory cells by FACS analysis, cells were stained with either FITC-CD11b

antibody (BD Biosciences) or FITC-CD11c antibody (BioLegend). The proper isotype controls were used in each case. The flow cytometry events were acquired with a MoFlo Legacy Cell Sorter (Beckman Coulter) and analyzed using the Summit Software.

Cell culture and *ex vivo* adipogenesis assays

Primary MEFs were derived from E13.5 animals and cultured in standard medium containing Dulbecco modified Eagle medium (DMEM) supplemented with 10% Fetal Bovine Serum (FBS), 50μg/ml streptomycin-50 U/ml penicillin (Sigma) and 2mM L-glutamine (Gibco). For the *ex vivo* adipogenesis assay, two-days post confluent primary MEFs were induced for adipocyte differentiation with standard medium supplemented with 1μM dexamethasone (Sigma), 10μg/ml insulin (Sigma) and 0,5mM 3-isobutil-1-methylxanthine (Sigma) (DIM). Fresh adipogenic medium was replenished every other day for 9 days (ChIP) or 13 days (mRNA levels). Adipocytes and undifferentiated MEFs were treated with 10 μg/μl mitomycin C (AppliChem) for 2 hours in serum-free DMEM to induce ICLs and were recovered for 6 hours in standard medium. For ATM or ATR kinase inhibitor assays, cells were pre-treated for 1 hour with 10 μM inhibitor (Millipore), followed by the addition of MMC in the presence of the inhibitor. *Ercc1*$^{-/-}$ MEFs were treated with ATMi for 48 hours prior collection and with 0.5 μM Rosiglitazone (SantaCruz Biotechnology) throughout differentiation.

References

- Andressoo, J.O., Hoeijmakers, J.H.J. and Mitchell, J.R. 2006. **Nucleotide excision repair disorders and the balance between cancer and aging**. Cell Cycle 5: 2886-8.
- Andressoo, J.O., Mitchell, J.R., de Wit, J., Hoogstraten, D., Volker, M., Toussaint, W., Speksnijder, E., Beems, R.B., van Steeg, H., Jans, J., de Zeeuw, C.I., Jaspers, N.G., Raams, A., Lehmann, A.R., Vermeulen, W., Hoeijmakers, J.H. and van der Horst, G.T. 2006b. **An Xpd mouse model for the combined xeroderma pigmentosum/Cockayne syndrome exhibiting both cancer predisposition and segmental progeria**. Cancer Cell 10: 121-32.
- Andressoo, J.O., Weeda, G., de Wit, J., Mitchell, J.R., Beems, R.B., van Steeg, H., van der Horst, G.T. and Hoeijmakers, J.H. 2009. **An Xpb mouse model for combined xeroderma pigmentosum and cockayne syndrome reveals progeroid features upon further attenuation of DNA repair**. Mol Cell Biol 29: 1276-90.
- Baker, R.G., Hayden, M.S. and Ghosh, S. 2011. **NF-κB, inflammation, and metabolic disease**. Cell Metab 13: 11-22.
- Chawla, A., Nguyen, K.D. and Goh, Y.P.S. 2011. **Macrophage-mediated inflammation in metabolic disease**. Nat Rev Immunol 11: 738-49.
- Ciccia, A. and Elledge, S.J. 2010. **The DNA damage response: making it safe to play with knives**. Mol Cell 40: 179-204.
- Citterio, E., Vermeulen, W. and Hoeijmakers, J.H.J. 2000. **Transcriptional healing**. Cell 101: 447-450.
- Clark, R.I., Tan, S.W.S., Pean, C.B., Roostalu, U., Vivancos, V., Bronda, K., Pilatova, M., Fu, J., Walker, D.W., Berdeaux, R., Geissmann, F. and Dionne, M.S. 2013. **MEF2 is an in vivo immune-metabolic switch**. Cell 155: 435-47.
- Clemmons, D.R. 2007. **Modifying IGF1 activity: an approach to treat endocrine disorders, atherosclerosis and cancer**. Nat Rev Drug Discov 6: 821-33.
- Colella, S., Nardo, T., Botta E., Lehmann, A.R. and Stefanini, M. 2000. **Identical mutations in the CSB gene associated with either Cockayne syndrome or the**

DeSanctis-cacchione variant of xeroderma pigmentosum. Hum Mol Genet 9: 1171-5.

- Coppe, J.P., Patil, C.K., Rodier, F., Sun, Y., Munoz, D.P., Goldstein, J., Nelson, P.S., Desprez, P.Y. and Campisi, J. 2008. **Senescence-associated secretory phenotypes reveal cell-nonautonomous function of oncogenic RAS and the p53 tumor suppressor**. PLoS Biol 6: 2853-68.
- D' Amours, D. and Jackson, S.P. 2002. **The Mre11 complex: at the crossroads of dna repair and checkpoint signalling**. Nat Rev Mol Cell Biol 3: 317-27.
- Dasika, G.K., Lin, S.C., Zhao, S., Sung, P., Tomkinson, A. and Lee, E.Y. 1999. **DNA damage-induced cell cycle checkpoints and DNA strand break repair in development and tumorigenesis**. Oncogene 18: 7883-99.
- Davalos, A.R., Kawahara, M., Malhotra, G.K., Schaum, N., Huang, J., Ved, U., Beausejour, C.M., Coppe, J.P., Rodier, F. and Campisi, J. 2013. **p53-dependent release of alarmin HMGB1 is a central mediator of senescent phenotypes**. J Cell Biol 201: 613-29.
- de Boer, E., Rodriguez, P., Bonte, E., Krijgsveld, J., Katsantoni, E., Heck, A., Grosveld, F. and Strouboulis, J. 2003. **Efficient biotinylation and single-step purification of tagged transcription factors in mammalian cells and transgenic mice**. Proc Natl Acad Sci USA 100: 7480-5.
- de Boer, J., Donker, I., de Wit, J., Hoeijmakers, J.H. and Weeda, G. 1998. **Disruption of the mouse xeroderma pigmentosum group D DNA repair/basal transcription gene results in preimplantation lethality**. Cancer Res 58: 89-94.
- de Boer, J. and Hoeijmakers, J.H.J. 2000. **Nucleotide excision repair and human syndromes**. Carcinogenesis 21: 453-460.
- de Boer, J., Andressoo, J.O., de Wit, J., Huijmans, J., Beems, R.B., van Steeg, H., Weeda, G., van der Horst, G.T., van Leeuwen, W., Themmen, A.P.N., Meradji, M. and Hoeijmakers, J.H. 2002. **Premature aging in mice deficient in DNA repair and transcription**. Science 296: 1276-9.
- de Vries, A., van Oostrom, C.T., Hofhuis, F.M., Dortant, P.M., Berg, R.J., de Gruijl, F.R., Wester, P.W., van Kreijl, C.F., Capel, P.J., van Steeg, H. and Verbeek, S.J. 1995. **Increased susceptibility to ultraviolet-B and carcinogens of mice lacking the DNA excision repair gene XPA**. Nature 377: 169-73.

- DiAngelo, J.R., Bland, M.L., Bambina, S., Cherry, S. and Birnbaum, M.J. 2009. **The immune response attenuates growth and nutrient storage in *Drosophila* by reducing insulin signalling**. Proc Natl Acad Sci USA 106: 20853-8.
- Ding, J., Miao, Z.H., Meng, L.H. and Geng, M.Y. 2006. **Emerging cancer therapeutic opportunities target DNA-repair systems**. Trends Pharmacol Sci 27: 338-44.
- Eichelbaum, K., Winter, M., Berriel Diaz, M., Herzig, S. and Krijgsveld, J. 2012. **Selective enrichment of newly synthesized proteins for quantitative secretome analysis**. Nat Biotechnol 30: 984-90.
- Elliott, B. and Jasin, M. 2002. **Double-strand breaks and translocations in cancer**. Cell Mol Life Sci 59: 373-85.
- Ermolaeva, M.A., Segref, A., Dakhovnik, A., Ou, H.L., Schneider, J.I., Utermohlen, O., Hoppe, T. and Schumacher, B. 2013. **DNA damage in germ cells induces an innate immune response that triggers systemic stress resistance**. Nature 501: 416-20.
- Ermolaeva, M.A. and Schumacher, B. 2014. **Systemic DNA damage responses: organismal adaptations to genome instability**. Trends Genet S0168-9525(13)00206-0. doi: 10.1016/j.tig.2013.12.001.
- Feldmeyer, L., Keller, M., Niklaus, G., Hohl, D., Werner, S. and Beer, H.D. 2007. **The inflammasome mediates UVB-induced activation and secretion of interleukin-1beta by keratinocytes**. Curr Biol 17: 1140-5.
- Fernandez-Capetillo, O., Lee, A., Nussenzweig, M. and Nussenzweig, A. 2004. **H2AX: the histone guardian of the genome**. DNA Repair 3: 959-67.
- Fiorenza, C.G., Chou, S.H. and Mantzoros, C.S. 2011. **Lipodystrophy: pathophysiology and advances in treatment**. Nat Rev Endoc 7: 137-50.
- Fong, Y.W., Inouye, C., Yamaguchi, T., Cattoglio, C., Grubisic, I. and Tjian, R. 2011. **A DNA repair complex functions as an Oct4/Sox2 coactivator in embryonic stem cells**. Cell 147: 120-31.
- Fong, Y.W., Cattoglio, C. and Tjian, R. 2013. **The intertwined roles of transcription and repair proteins**. Mol Cell 52: 291-302.
- Fousteri, M., Vermeulen, W., van Zeeland, A.A. and Mullenders, L.H. 2006. **Cockayne syndrome A and B proteins differentially regulate recruitment of**

chromatin remodelling and repair factors to stalled RNA polymerase II in vivo. Mol Cell 23: 471-82.

- Freund, A., Orjalo, A.V., Desprez, P.Y. and Campisi, J. 2010. **Inflammatory networks during cellular senescence: causes and consequences**. Trends Mol Med 16: 238-46.
- Friedberg, E.C. 2001. **How nucleotide excision repair protects against cancer**. Nat Rev Cancer 1: 22-33.
- Garinis, G.A., Mitchell, J.R, Moorhouse, M.J. *et al* 2005. **Transcriptome analysis reveals cyclobutane pyrimidine dimmers as a major source of UV-induced DNA breaks**. Embo J 24: 3952-62.
- Garinis, G.A., van der Horst, G.T.J., Vijg, J. and Hoeijmakers, J.H.J. 2008. **DNA damage and ageing: new-age ideas for an age-old problem**. Nat Cell Biol 10:1241-7.
- Garinis, G.A., Uittenboogaard, L.M., Stachelscheid, H., Fousteri, M., van Ijcken, W., Breit, T.M., van Steeg, H., Mullenders, L.H.F., van der Horst, G.T.J., Bruening, J.C., Niessen, C.M., Hoeijmakers, J.H.J. and Schumacher, B. 2009. **Persistent transcription-blocking DNA lesions trigger somatic growth attenuation associated with longevity**. Nat Cell Biol 11: 604-15.
- Garinis, G.A. and Schumacher, B. 2009. **Transcription-blocking DNA damage in aging and longevity**. Cell Cycle 8: 2134-5.
- Gasser, S., Orsulic, S., Brown, E.J. and Raulet, D.H. 2005. **The DNA damage pathway regulates innate immune system ligands of the NKG2D receptor**. Nature 436: 1186-90.
- Gesta, S., Tseng, Y.H. and Kahn, R.C. 2007. **Developmental origin of fat: tracking obesity to its source**. Cell 131: 242-56.
- Han, J., Lee, J.E., Jin, J., Lim, J.S., Oh, N., Kim, K., Chang, S.I., Shibuya, M., Kim, H. and Koh, G.Y. 2011. **The spatiotemporal development of adipose tissue**. Development 138: 5027-37.
- Hanawalt, P.C. 2002. **Subpathways of nucleotide excision repair and their regulation**. Oncogene 21: 8949-56.
- Harada, Y.N., Shiomi, N., Koike, M., Ikawa, M., Okabe, M., Hirota, S., Kitamura, Y., Kitagawa, M., Matsunaga, T., Nikaido, O. and Shiomi, T. 1999. **Postnatal growth failure, short life span, and early onset of cellular senescence and**

subsequent immortalization in mice lacking the xeroderma pigmentosum group G protein. Mol Cell Biol 19: 2366-72.

- Hasty, P., Campisi, J., Hoeijmakers, J., van Steeg, H. and Vijg, J. 2003. **Aging and genome maintenance: lessons from the mouse?** Science 299: 1355-9.
- Hegele, R.A., Joy, T.R., Al-Attar, S.A. and Rutt, B.K. 2007. **Thematic review series: Adipocyte biology. Lipodystrophies: windows on adipose biology and metabolism**. J Lipid Res 48: 1433-44.
- Herrero, L., Shapiro, H., Nayer, A., Lee, J. and Shoelson, S.E. 2007. **Inflammation and adipose tissue macrophages in lipodystrophic mice**. Proc Natl Acad Sci USA 107: 240-5.
- Hoeijmakers, J.H.J. 2001. **Genome maintenance mechanisms for preventing cancer**. Nature 411: 366-74.
- Hotamisligil, G.S., Shargill, N.S. and Spiegelman, B.M. 1993. **Adipose expression of tumour necrosis factor-alpha: direct role in obesity-linked insulin resistance**. Science 259: 87-91.
- Hotamisligil, G.S., Murray, D.L., Choy, L.N. and Spiegelman, B.M. 1994. **Tumour necrosis factor alpha inhibits signaling from the insulin receptor**. Proc Natl Acad Sci USA 91: 4854-8.
- Hotamisligil, G.S. 2006. **Inflammation and metabolic disorders**. Nature 444: 860-7.
- Jaspers, N.G.H., Raams, A., Silengo, M.C., Wijgers, N., Niedernhofer, L.J., Robinson, A.R., Giglia-Mari, G., Hoogstraten, D., Kleijer, W.J., Hoeijmakers, J.H.J. and Vermeulen, W. 2007. **First reported patient with human ERCC1 deficiency has cerebro-oculo-facio-skeletal syndrome with a mild defect in nucleotide excision repair and severe developmental failure**. A J Hum Genet 80: 457-66.
- Jones, J.R., Barrick, C., Kim, K.A., Lindner, J., Blondeau, D., Fujimoto, Y., Shiota, M., Kesterson, R.A., Kahn, B.B. and Magnuson, M.A. 2005. **Deletion of PPARgamma in adipose tissues of mice protects against high fat diet-induced obesity and insulin resistance**. Proc Natl Acad Sci USA 102: 6207-12.
- Kadowaki, T., Yamauchi, T., Kubota, N., Hara, K., Ueki, K. and Tobe, K. 2006. **Adiponectin and adiponectin receptors ininsulin resistance, diabetes, and the metabolic syndrome**. J Clin Invest 116: 1784-92.

- Kamenisch, Y., Fousteri, M., Knoch, J., von Thaler, N.K., Fehrenbacher, B., Kato, H., Becker, T., Dolle, M.E.T., Kuiper, R. *et al*. 2010. **Proteins of nucleotide and base excision repair pathways interact in mitochondria to protect from loss of subcutaneous fat, a hallmark of ageing**. J Exp Med 207: 379-90.
- Kamileri, I., Karakasilioti, I. and Garinis, G.A. 2012. **Nucleotide excision repair: new tricks with old bricks**. Trends Genet 28: 566-73.
- Kamileri, I., Karakasilioti, I., Sideri, A., Kosteas, T., Tatarakis, A., Talianidis, I. and Garinis, G.A. 2012b. **Defective transcription initiation causes postnatal growth failure in a mouse model of nucleotide excision repair (NER) progeria**. Proc Natl Acad Sci USA 109: 2995-3000.
- Karagiannides, I., Tchkonia, T., Dobson, D.E., Steppan, C.M., Cummins, P., Chan, G., Salvatori, K., Hadzopoulou-Cladaras, M. and Kirkland, J.L. 2001. **Altered expression of C/EBP family members results in decreased adipogenesis with aging**. Am J Physiol Regul Integr Comp Physiol 280: R1772-R1780.
- Karagiannides, I., Thomou, T., Tchkonia, T., Pirtskhalava, T., Kypreos, K.E., Cartwright, A., Dalagiorgou, G., Lash, T.L., Farmer, S.R., Timchenko, N.A. and Kirkland, J.L. 2006. **Increased CUG triplet repeat-binding protein-1 predisposes to impaired adipogenesis with aging**. J Biol Chem 281: 23025-33.
- Kennedy, A.J., Ellacott, K.L.J., King, V.L. and Hasty, A.H. 2010. **Mouse models of the metabolic syndrome**. Dis Model Mech 3: 156-66.
- Kenyon, C. 2006. **The plasticity of aging: insights from long-lived mutants**. Cell 120: 449-60.
- Kenyon, C.J. 2010. **The genetics of ageing**. Nature 464: 504-12.
- Khazen, W., M'bika, J.P., Tomkiewicz, C., Benelli, C., Chany, C., Achour, A. and Forest, C. 2005. **Expression of macrophage-selective markers in human and rodent adipocytes**. FEBS lett 579: 5631-4.
- Kim, S., Huang, L.W., Snow, K.J., Ablamunits, V., Hasham, M.G., Young, T.H., Paulk, A.C., Richardson, J.E., Affourtit, J.P., Shalom-Barak, T., Bult, C.J. and Barak, Y. 2007. **A mouse model of conditional lipodystrophy**. Proc Natl Acad Sci USA 104: 16627-32.
- Kimura, I., Moritani, Y. and Tanizaki, Y. 1973. **Basophils in bronchial asthma with reference to reagin-type allergy**. Clin Allergy 3: 195-202.

- Kirkwood, T.B. 2005. **Understanding the odd science of aging**. Cell 120: 437-47.
- Kottemann, M.C. and Smogorzewska, A. 2013. **Fanconi anemia and the repair of Watson and Crick crosslinks**. Nature 493: 356-63.
- Lagerwerf, S., Vrouwe, M.G., Overmeer, R.M., Fousteri, M. and Mullenders, L.H. 2011. **DNA damage response and transcription**. DNA repair 10: 743-50.
- Laine, J.P. and Egly, J.M. 2006. **Initiation of DNA repair mediated by a stalled RNA polymerase IIO**. Embo J 25: 387-97.
- Laugel, V., Dalloz, C., Durand, M., Sauvanaud, F., Kristensen, U., Vincent, M.C., Pasquier, L., Odent, S., Cormier-Daire, V., Gener, B., Tobias, E.S., Tolmie, J.L. *et al*. 2010. **Mutation update for the CSB/ERCC6 and CSA/ERCC8 genes involved in Cockayne syndrome**. Hum Mutat 31: 113-26.
- Le May, N., Mota-Fernandes, D., Velez-Cruz, R., Iltis, I., Biard, D. and Egly, J.M. 2010. **NER factors are recruited to active promoters and facilitate chromatin modification for transcription in the absence of exogenous genotoxic attack**. Mol Cell 38: 54-66.
- Mao, J., Yang, T., Gu, Z., Heird, W.C., Finegold, M.J., Lee, B. and Wakil, S.J. 2009. **aP2-Cre-mediated inactivation of acetyl-CoA carboxylase 1 causes growth retardation and reduced lipid accumulation in adipose tissues**. Proc Natl Acad Sci USA 106: 17576-81.
- Masutani, C., Sugasawa, K., Yanagisawa, J., Sonoyama, T., Ui, M., Enomoto, T., Takio, K., Tanaka, K., van der Spek, P.J., Bootsma, D. *et al*. 1994. **Purification and cloning of a nucleotide excision repair complex involving the xeroderma pigmentosum group C protein and a human homologue of yeast RAD23**. Embo J 13: 1831-43.
- Medzhitov, R. 2010. **Inflammation 2010: new adventures of an old flame**. Cell 140: 771-6.
- Miyake, Y. and Yamasaki, S. 2012. **Sensing necrotic cells**. Adv Exp Med Biol 738: 144-52.
- Moser, J., Kool, H., Giakzidis, I., Caldecott, K., Mullenders, L.H. and Fousteri, M. 2007. **Sealing of chromosomal DNA nicks during nucleotide excision repair requires XRCC1 and DNA ligase III alpha in a cell cycle-specific manner**. Mol Cell 27: 311-23.

- Muse, G.W., Gilchrist, D.A., Nechaev, S., Shah, R., Parker, J.S., Grissom, S.F., Zeitlinger, J. and Adelman, K. 2007. **RNA polymerase is poised for activation across the genome**. Nat Genet 39: 1507-11.
- Nakane, H., Takeuchi, S., Yuba, S., Saijo, M., Nakatsu, Y., Murai, H., Nakatsuru, Y., Ishikawa, T., Hirota, S., Kitamura, Y. *et al*. 1995. **High incidence of ultraviolet-B or chemical-carcinogen-induced skin tumours in mice acking the xeroderma pigmentosum group A gene**. Nature 377: 165-8.
- Niedernhofer, L.J., Odijk, H., Budzowska, M., van Drunen, E., Maas, A., Theil, A.F., de Wit, J., Jaspers, N.G.J., Beverloo, H.B., Hoeijmakers, J.H.J. and Kanaar, R. 2004. **The structure-specific endonuclease Ercc1-Xpf is required to resolve DNA interstrand cross-link-induced double-strand breaks**. Mol Cell Biol 24: 5776-87.
- Niedernhofer, L.J., Garinis, G.A., Raams, A., Lalai, A.S., Robinson, A.R., Appeldoorn, E., Odijk, H., Oostendorp, R., Ahmad, A., van Leeuwen, W., Theil, A.F., Vermeulen, W., van der Horst, G.T.J., Meineke, P., Kleijer, W.J., Vijg, J., Jaspers, N.G.J. and Hoeijmakers, J.H.J. 2006. **A new progeroid syndrome reveals that genotoxic stress suppresses the somatotroph axis**. Nature 444: 1038-43.
- Nishi, R., Okuda, Y., Watanabe, E., Mori, T., Iwai, S., Masutani, C., Sugasawa, K. and Hanaoka, F. 2005. **Centrin 2 stimulates nucleotide excision repair by interacting with xeroderma pigmentosum group C protein**. Mol Cell Biol 25: 5664-74.
- Nishimura, S., Manabe, I., Nagasaki, M., Hosoya, Y., Yamashita, H., Fujita, H., Ohsugi, M., Tobe, K., Kadowaki, T., Nagai, R. and Sugiura, S. 2007. **Adipogenesis in obesity requires cose interplay between differentiating adipocytes, stromal cells, and blood vessels**. Diabetes 56: 1517-26.
- Oh, K.S., Khan, S.G., Jaspers, N.J., Raams, A., Ueda, T., Lehmann, A., Friedmann, P.S., Emmert, S., Gratchev, A., Lachlan, K., Lucassan, A., Baker, C.C. and Kraemer, K.H. 2006. **Phenotypic heterogeneity in the XPB DNA helicase gene (ERCC3): xeroderma pigmentosum without and with cockayne syndrome**. Hum Mutat 27: 1092-103.

- Oksenych, V., Bernardes de Jesus, B., Zhovmer, A., Egly, J.M. and Coin, F. 2009. **Molecular insights into the recruitment of TFIIH to sites of DNA damage**. Embo J 28: 2971-80.
- Overmeer, R.M., Moser, J., Volker, M., Kool, H., Tomkinson, A.E., van Zeeland, A.A., Mullenders, L.H. and Fousteri, M. 2011. **Replication protein A safeguards genome integrity by controlling NER incision events**. J Cell Biol 192: 401-15.
- Ouchi, N., Parker, J.L., Lugus, J.J. and Walsh, K. 2011. **Adipokines in inflammation and metabolic disease**. Nat Rev Immunol 11: 85-97.
- Park, J.S., Svetkauskaite, D., He, Q., Kim, J.Y., Strassheim, D., Ishizaka, A. and Abraham, E. 2004. **Involvement of Toll-like receptors 2 and 4 in cellular activation by high mobility group box 1 protein**. J Biol Chem 279: 7370-7.
- Perissi, V., Jepsen, K., Glass, C.K. and Rosenfeld, M.G. 2010. **Deconstructing repression: evolving models of co-repressor action**. Nat Rev Genet 11: 109-23.
- Rodier, F., Coppe, J.P., Patil, C.K., Hoeijmakers, W.A.M., Munoz, D.P., Raza, S.R., Freund, A., Campeau, E., Davalos, A.R. and Campisi, J. 2009. **Persistent DNA damage signalling triggers senescence-associated inflammatory cytokine secretion**. Nat Cell Biol 11: 973-9.
- Rodier, F., Munoz, D.P., Teachenor, R., Chu, V., Le, O., Bhaumik, D., Coppe, J.P., Campeau, E., Beausejour, C.M., Kim, S.H., Davalos, A.R. and Campisi, J. 2011. **DNA-SCARS: distinct nuclear structures that sustain damage-induced senescence growth arrest and inflammatory cytokine secretion**. J Cell Sci 124: 68-81.
- Rosen, E.D. and MacDougald, O.A. 2006. **Adipocyte differentiation from inside out**. Nat Rev Mol Cell Biol 7: 885-6.
- Rosen, E.D. and Spiegelman, B.M. 2006. **Adipocytes as regulators of energy balance and glucose homeostastis**. Nature 444: 847-53.
- Saijo, M. 2013. **The role of Cockayne syndrome group A (CSA) protein in transcription-coupled nucleotide excision repair**. Mech Ageing Dev 134: 196-201.
- Satir, P., Pedersen, L.B. and Christensen, S.T. 2010. **The primary cilium at a glance**. J Cell Sci 123: 499-503.
- Sato, K., Ishiai, M., Toda, K., Furukoshi, S., Osakabe, A., Tachiwana, H., Takizawa, Y., Kagawa, W., Kitao, H., Dohmae, N., Obuse, C., Kimura, H.,

Takata, M. and Kurumizaka, H. 2012. **Histone chaperone activity of Fanconi Anemia proteins, FANCD2 and FANCI, is required for DNA crosslink repair**. Embo J 31: 3524-36.

- Schwertman, P., Lagarou, A., Dekkers, D.H., Raams, A., van der Hoek, A.C., Laffeber, C., Hoeijmakers, J.H., Demmers J.A., Fousteri, M., Vermeulen, W. and Marteijn, J.A. 2012. **UV-sensitive syndrome protein UVSSA recruits USP7 to regulate transcription-coupled repair**. Nat Genet 44: 598-602.
- Schumacher, B., Garinis, G.A. and Hoeijmakers, J.H. 2008. **Age to survive: DNA damage and ageing**. Trends Genet 24: 77-85.
- Sepe, A., Tchkonia, T., Thomou, T., Zamboni, M. and Kirkland, J.L. 2011. **Aging and regional differences in fat cell progenitors – a mini-review**. Gerontology 57: 66-75.
- Soriani, A., Zingoni, A., Cerboni, C., Iannitto, M.L., Ricciardi, M.R., Di Gialleonardo, V., Cippitelli, M., Fionda, C., Petrucci, M.T., Guarini, A., Foa, R. and Santoni, A. 2009. **ATM-ATR – dependent up-regulation of DNAM-1 and NKG2D ligants on multiple myeloma cells by therapeutic agents results in enhanced NK-cell susceptibility and is associated with a senescent phenotype**. Blood 113: 3503-11.
- Spivak, G., Itoh, T., Matsunaga, T., Nakaido, O., Hanawalt, P. and Yamaizumi, M. 2002. **Ultra-violet sensitive syndrome cells are defective in transcription-coupled repair of cyclobutane pyrimidine dimers**. DNA Repair 1: 629-43.
- Steppan, C.M., Bailey, S.T., Bhat, S., Brown, E.J., Banerjee, R.R., Wright, C.M., Patel, H.R., Ahima, R.S. and Lazar, M.A. 2001. **The hormone resistin links obesity to diabetes**. Nature 409: 307-12.
- Straus, D.S. and Glass, C.K. 2007. **Anti-inflammatory actions of PPAR ligands: new insights on cellular and molecular mechanisms**. Trends Immunol 28: 551-8.
- Sun, K., Kusminski, C.M. and Scherer, P.E. 2011. **Adipose tissue remodelling and obesity**. J Clin Invest 121: 2094-101.
- Tang, W., Zeve, D., Suh, J.M., Bosnakovski, D, Kyba, M., Hammer, R.E., Tallquist, M.D. and Graff, J.M. 2008. **White fat progenitor cells reside in the adipose vasculature**. Science 322: 583-6.

- Tchkonia, T., Pirtskhalava, T., Thomou, T., Cartwright, M.J., Wise, B., Karagiannides, I., Shpilman, A., Lash, T.L., Becherer, J.D. and Kirkland, J.L. 2007. **Increased TNFalpha and CCAAT/enhancer-binding protein homologous protein with aging predispose preadipocytes to resist adipogenesis**. Am J Physiol Endocrinol Metab 293: E1810-E1819. doi: 10.1152/ajpendo.00295.2007.
- Tchkonia, T., Morbeck, D.E., von, Zglinicki, T., van Deursen, J., Lustgarden, J., Scrable, H., Khosla, S., Jensen, M.D. and Kirkland, J.L. 2010. **Fat tissue, aging, and cellular senescence**. Aging Cell 9: 667-84.
- Theil, A.F., Nonnekens, J., Steurer, B., Mari, P.O., de Wit, J., Lemaitre, C., Marteijn, J.A., Raams, A., Maas, A., Vermeij, M., Essers, J., Hoeijmakers, J.H., Giglia-Mari, G. and Vermeulen, W. 2013. **Disruption of TTDA results in complete nucleotide excision repair deficiency and embryonic lethality**. PLoS Genet 9: e1003431. doi: 10.1371/journal.pgen.1003431.
- Tian, M., Shinkura, R., Shinkura, N. and Alt, F.W. 2004. **Growth retardation, early death, and DNA repair defects in mice deficient for the nucleotide excision repair enzyme XPF**. Mol Cell Biol 24: 1200-5.
- Tilstra, J.S., Robinson, A.R., Wang, J., Gregg, S.Q., Clauson, C.L., Reay, D.P., Nasto, L.A., St Croix, C.M., Usas, A., Vo, N., Huard, J., Clemens, P.R., Stolz, D.B., Guttridge, D.C., Watkins, A.C., Garinis, G.A., Wang, Y., Niedernhofer, L.J. and Robbins, P.D. 2012. **NF-κB inhibition delays DNA damage-induced senescence and aging in mice**. J Clin Invest 122: 2601-12.
- van der Horst, G.T., van Steeg, H., Berg, R.J.W., van Gool, A.J., de Wit, J., Weeda, G., Morreau, H., Beems, R.B., van Kreijl, C.F., de Gruijl, F.R., Bootsma, D. and Hoeijmakers, J.H.J. 1997. **Defective transcription-coupled repair in cockayne syndrome B mice is associated with skin cancer predisposition**. Cell 89: 425-35.
- van der Pluijm, I., Garinis, G.A., Brandt, R.M.C., Gorgels, T.G.M.F., Wijnhoven, S.W., Diderich, K.E.M., de Wit, J., Mitchell, J.R., van Oostrom, C., Beems, R., Niedernhofer, L.J., Velasco, S., Friedberg, E.C., Tanaka, K., van Steeg, H., Hoeijmakers, J.H.J., van der Horst, G.T.J. 2007. **Impaired genome maintenance suppresses the growth hormone – insulin-like growth factor 1 axis in mice with Cockayne Syndrome**. PLoS Biol 5: e2. doi:10.1371/journal.pbio.0050002.

- van Gent, D.C., Hoeijmakers, J.H.J. and Kanaar, R. 2001. **Chromosomal stability and the DNA double-stranded break connection**. Nat Rev Genet 2: 196-206.
- Verhagen-Oldenampsen, J.H., Haanstra, J.R., van Strien, P.M., Valkhof, M., Touw, I.P. and von Lindern, M. 2012. **Loss of ercc1 results in a time- and dose-dependent reduction of proliferating early hematopoietic progenitors**. Anemia, doi:10.1155/2012/783068.
- Wang, Y., Lam, K.S., Kraegen, E.W., Sweeney, G., Zhang, J., Tso, A.W., Chow, W.S., Wat, N.M., Xu, J.Y., Hoo, R.L. and Xu, A. 2007. **Lipocalin-2 is an inflammatory marker closely associated with obesity, insulin resistance, and hyperglycaemia in humans**. Clin Chem 53: 34-41.
- Weeda, G., Donker, I., de Wit, J., Morreau, H., Janssens, R., Vissers, C.J., Nigg, A., van Steeg, H., Bootsma, D. and Hoeijmakers, J.H.J. 1997. **Disruption of mouse *ERCC1* results in a novel repair syndrome with growth failure, nuclear abnormalities and senescence**. Curr Biol 7: 427-39.
- West, S.C. 2003. **Molecular views of recombination proteins and their control**. Nat Rev Mol Cell Biol 4: 435-45.
- Wu, Z.H., Shi, Y., Tibbetts, R.S. and Miyamoto, S. 2006. **Molecular linkage between the kinase ATM and NF-kappaB signaling in response to genotoxic stimuli**. Science 311: 1141-6.
- Yang, D.Q. and Kastan, M.B. 2000. **Participation of ATM in insulin signalling through phosphorylation of eIF-4E-binding protein 1**. Nat Cell Biol 2: 893-8.
- Yang, D.Q., Halaby, M.J., Li, Y., Hibma, J.C. and Burn, P. 2011. **Cytoplasmic ATM protein kinase: an emerging therapeutic target for diabetes, cancer and neuronal degeneration**. Drug Discov Today 16: 332-8.